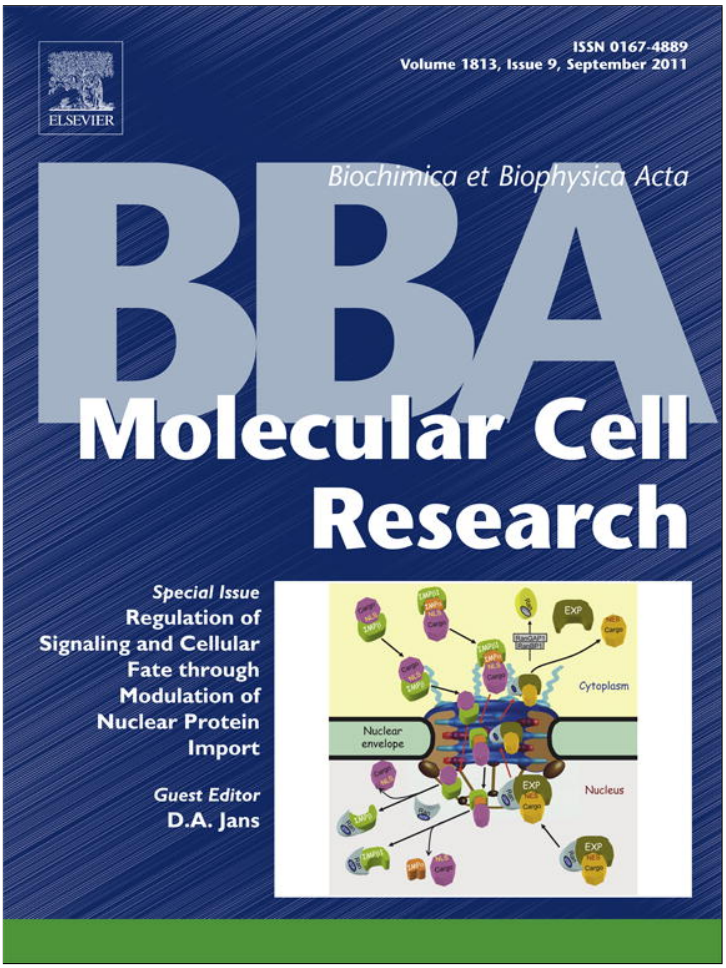

Biochimica et Biophysica Acta 1813 (2011) 1607–1618

Contents lists available at ScienceDirect

Biochimica et Biophysica Acta

journal homepage: www.elsevier.com/locate/bbamcr

Review

Single molecule studies of nucleocytoplasmic transport ☆

Li-Chun Tu, Siegfried M. Musser *

Department of Molecular and Cellular Medicine, College of Medicine, Texas A&M Health Science Center, College Station, TX 77843, USA

ARTICLE INFO

Article history:
Received 1 June 2010
Received in revised form 18 October 2010
Accepted 8 December 2010
Available online 16 December 2010

Keywords:
Nuclear pore complex
Nuclear transport
Single molecule fluorescence

ABSTRACT

Molecular traffic between the cytoplasm and the nucleoplasm of eukaryotic cells is mediated by nuclear pore complexes (NPCs). Hundreds, if not thousands, of molecules interact with and transit through each NPC every second. The pore is blocked by a permeability barrier, which consists of a network of intrinsically unfolded polypeptides containing thousands of phenylalanine–glycine (FG) repeat motifs. This FG-network rejects larger molecules and admits smaller molecules or cargos bound to nuclear transport receptors (NTRs). For a cargo transport complex, minimally consisting of a cargo molecule plus an NTR, access to the permeability barrier is provided by interactions between the NTR and the FG repeat motifs. Numerous models have been postulated to explain the controlled accessibility and the transport characteristics of the FG-network, but the amorphous, flexible nature of this structure has hindered characterization. A relatively recent development is the ability to monitor the real-time movement of single molecules through individual NPCs via single molecule fluorescence (SMF) microscopy. A major advantage of this approach is that it can be used to continuously monitor a series of specific molecular interactions in an active pore with millisecond time resolution, which therefore allows one to distinguish between kinetic and thermodynamic control. Novel insights and prospects for the future are outlined in this review. This article is part of a Special Issue entitled: Regulation of Signaling and Cellular Fate through Modulation of Nuclear Protein Import.

1. Introduction

In eukaryotic cells, the genome is sheltered in the nucleus, an organelle surrounded by a double-membrane system called the nuclear envelope (NE). Nuclear pore complexes (NPCs) embedded in the NE control molecular traffic between the nucleus and the cytoplasm. Substrates (cargos) that must enter or exit the nucleus include an extensive array of proteins and nucleic acids. Hence, in all eukaryotic cells, the proper functioning of NPCs is essential. The mass flow through NPCs in proliferating HeLa cells is estimated to be 10–20 MDa·NPC^{-1} s^{-1} [1]. The structural and functional properties of NPCs are highly conserved, though they range in size from ~66 MDa in yeast to ~125 MDa in metazoans [2–4]. The large molecular mass of NPCs and their capability of mediating massive transport fluxes are reflected in a large pore, which is capable of allowing the passage of cargos up to ~40 nm (~25 MDa) [5]. The effective pore size depends on the size and surface characteristics of a particular molecule or complex. The traditional rule is that molecules larger than ~20–40 kDa need to be specifically recognized in order to be transported ("signal-dependent transport"), whereas molecules smaller than this mass freely transit the NPC without specific recognition ("signal-independent transport"). For example, small metabolites and even small proteins freely equilibrate between the cytoplasmic and nucleoplasmic compartments. However, although molecular size is an important constraint determining NPC permeability, molecular surface properties are also crucial since transport receptors of ~100 kDa easily penetrate the NPC, and minor changes to the surface of a protein can dramatically affect its NPC permeability [6]. Further, it has recently been suggested that electrostatic interactions contribute significantly to NPC permeability [7]. How the factors governing cargo selectivity and how the effective pore size can rapidly change to allow the simultaneous transport of many different cargos in both directions are important fundamental issues that remain unresolved. Central to these issues are the properties of the amorphous material that occludes the central pore.

Some recent work has focused on directly observing individual molecules transiting the NPC in real time under physiological transport conditions. Such studies allow previously unaddressable questions to be probed and promise a new level of understanding. There are numerous recent reviews that detail the structural and functional properties of NPCs (for example, see [8–11]). The reader is directed to these for more exhaustive lists of references on this material. In the next few sections, we outline the basic framework of nucleocytoplasmic transport necessary for understanding the

Abbreviations: NPC, nuclear pore complex; Nup, nucleoporin; NE, nuclear envelope; SMF, single molecule fluorescence; NTR, nuclear transport receptor; S/N, signal-to-noise ratio; fps, frames per second; smFRET, single molecule fluorescence resonance energy transfer

☆ This article is part of a Special Issue entitled: Regulation of Signaling and Cellular Fate through Modulation of Nuclear Protein Import.

* Corresponding author. Tel.: +1 979 862 4128; fax: +1 979 847 9481.
E-mail address: smusser@tamu.edu (S.M. Musser).

0167-4889/$ – see front matter © 2011 Elsevier B.V. All rights reserved.
doi:10.1016/j.bbamcr.2010.12.011

implications of single molecule experiments. After this introduction, we focus on single molecule investigations of nuclear transport, and what these studies can, and are expected to, tell us.

2. NPC structure

Structural elements of the NPC extend ~200 nm along the transport axis and ~120 nm laterally. The central pore has inner dimensions of ~60–90 nm in length and ~45–50 nm at its narrowest width. Flexible filaments extend ~50 nm into the cytoplasm. Additional filaments extend at least 50–100 nm into the nucleoplasm, and are attached to the distal ring forming the nuclear basket [3,4,108,109,110,111]. The NPC is composed of over 450 individual proteins collectively termed nucleoporins (Nups) [12,13]. Because the NPC has octagonal rotational symmetry, it is assumed that each Nup is present in each NPC in an integer multiple of eight copies [2,12]. Consequently, there are only approximately 30 distinct Nups in yeast and metazoan cells, which are unfortunately described by different nomenclatures. The mammalian nomenclature is used in this review. The Nups are classified into two major subtypes, those that contain phenylalanine–glycine repeats (FG-Nups) and those that do not. About one-third to one-half of the Nups are FG-Nups and these contain five different flavors of FG-repeats, FG, FxFG, GLFG, SAFG, or PSFG [14]. Each FG-Nup contains a globular, anchoring domain that integrates into the NPC scaffold. The FG-containing portions, which consist of FG motifs typically spaced by 10–20 residue long spacer regions that are largely hydrophilic [15], account for ~12% of the total NPC mass [16]. These unique primary sequences result in intrinsically (or natively) unfolded polypeptides that interact and assemble into ill-defined structures that are highly hydrated and deformable, and yet provide a semi-permeable barrier. The ensemble FG-Nup structure has been variously termed a phase, a gel, spaghetti, a polymer brush, or simply a meshwork or network [1,17–21]. These descriptive terms suggest various physical properties, most or all of which are likely valid under certain conditions. What is unclear is which term best describes the *in vivo* properties of the barrier. A composite picture is feasible [14]. In this review, we will use the term FG-network to reflect the intermingling of the various FG polypeptides, and the fact that together these molecules are essential for the selective barrier of the NPC.

3. Nuclear transport

Cargos transit through NPCs via one of two pathways, the signal-dependent or the signal-independent pathway (for reviews, see [22–26]). The signal-independent pathway is a passive (energy independent) process. Signal-independent cargos equilibrate through NPCs dependent on their intrinsic ability to enter the FG-network and their concentration gradient across the NE. In contrast, signal-dependent cargos must be specifically recognized by receptors, and energy is required to provide transport directionality and to accumulate against a concentration gradient. The extent for cargos which the two pathways overlap remains a controversial issue [21,27,28].

Signal-dependent nuclear transport relies on two fundamental properties. The cargo must contain the appropriate signal (either a linear sequence, or a signal patch) [29], and, once recognized, the cargo must be able to penetrate the FG-network permeability barrier. These functions are provided by soluble nuclear transport receptors (NTRs). NTRs interact with the FG motifs in the FG-network, and allow bound cargos to penetrate the pore. The largest class of NTRs is the importin β (Imp β) superfamily, which includes both importins (which promote import) and exportins (which promote export). Importins and exportins are also known collectively as karyopherins. NTRs contain binding sites for nuclear localization sequences (NLSs), responsible for nuclear import, or nuclear export sequences (NESs), for nuclear export. In some cases, adaptors are used to bridge the interaction between a cargo's signal sequence and its cognate NTR. For example, members of the importin α (Imp α) family contain an NLS-binding motif and an Imp β binding domain, and thus allow for independently regulated transport pathways [22,23]. At least seven types of Imp α have been identified in higher eukaryotes [30,31].

Signal-dependent cargo molecules migrate with NTRs through the NPC (Fig. 1). In the case of import, a minimal transport complex is a heterodimeric complex consisting of a cargo molecule and an NTR (e.g., Imp β). If Imp α is used by a particular import pathway, the transport complex is the heterotrimeric Imp β/Imp α/cargo complex. Export complexes are similarly composed of an NTR and cargo molecule, with one important difference. Export complexes are stabilized by the GTP-bound form of Ran, RanGTP [32,33]. Import and export complexes are disassembled after successful transport, both to release the free cargo molecule, and to recycle the NTR(s) for another round of transport. In the case of import, the binding of RanGTP to importins results in complex disassembly. In contrast, export complexes with RanGTP are stable, and activation of the RanGTPase and complex disassembly minimally require RanGAP and a Ran binding protein (e.g., RanBP1 or RanBP2) [34–37]. Efficient dissociation of Imp β1/RanGTP complexes additionally requires Imp α [34,35,37]. RanGDP is recycled back to the nucleus with NTF2 [38].

Factors that promote import complex disassembly are found on the nucleoplasmic side of the pore and factors that promote export complex disassembly are found on the cytoplasmic filaments. For example, Nup50, found on the nucleoplasmic side of the pore, promotes dissociation of Imp α/cargo complexes [39–42]. Nup358 (also known as RanBP2), the major component of the cytoplasmic filaments, binds SUMOylated RanGAP and contains RanBP1 homology domains, which bind to Ran [43,44]. Thus, transport complex disassembly is envisioned to occur at the NPC at the end of, or concomitant with, the transport process. A critical component driving the overall direction of signal-dependent nuclear transport is the RanGTP gradient. Since RanGTP is required both for import complex disassembly and export complex assembly, the RanGTP concentration is high in the nucleus. The presence of RanGAP in the cytoplasm insures that the RanGTP concentration is low in this compartment. In the nucleoplasm, RanGEF, a guanine nucleotide exchange factor, insures that RanGTP is regenerated from RanGDP in the nucleus [45]. Reversal of the RanGTP concentration gradient reverses the direction of transport [46].

4. Single molecule fluorescence approaches

Single molecule fluorescence (SMF) approaches have many benefits, but a primary advantage of such methods for studying complex biological reactions is the ability to continuously monitor an individual molecule as it migrates through a complex milieu and as it encounters many different molecules and nanoenvironments. In bulk experiments, the details of many brief interactions are simply lost due to ensemble averaging. Most SMF experiments to date have taken advantage of the fact that the molecules of interest are tethered at an interface coinciding with the image plane and/or the reactions under study can be imaged at video rates (30 frames per second or fps) or slower. It is technically simpler to collect more photons with longer exposure times, and hence, greater sensitivity and better signal-to-noise ratios (S/Ns) are observed under these conditions. However, bulk nuclear transport rates predict that NPCs can transport hundreds to thousands of molecules per second [1,20], suggesting individual transport times of ≤10 ms. Further, at 100 fps, diffusing molecules can migrate through a 2D image plane between successive frames. Thus, imaging a dynamic process, such as single molecules diffusing to, interacting with, and leaving NPCs, is a challenging endeavor. Fortunately, modern lasers and high-speed, highly sensitive cameras provide the excitation power and emission sensitivities necessary for

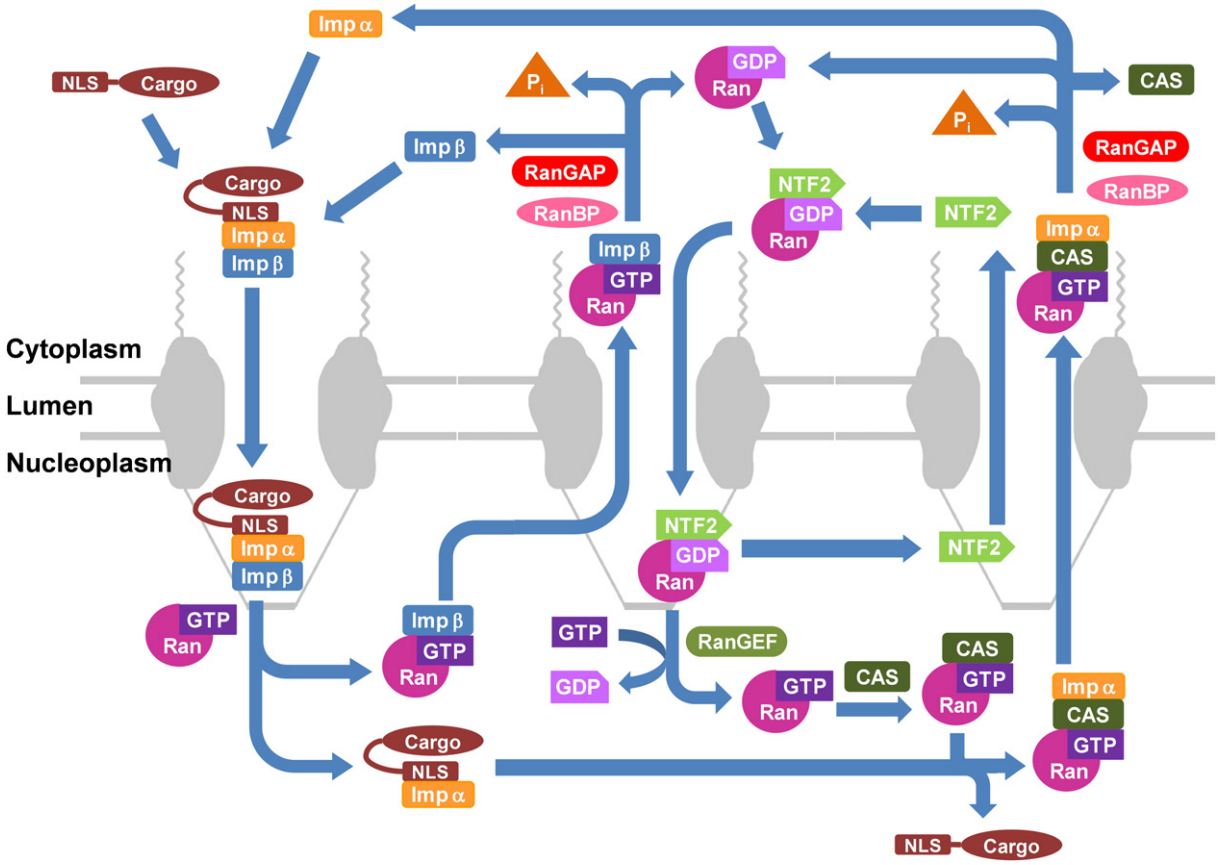

Fig. 1. Nuclear protein import and export pathways. The NTRs Imp β, NTF2, and CAS interact with FG-repeats and thereby mediate translocation through the FG-network permeability barrier (not shown). Starting at the top left, one import pathway is that a cargo molecule is recognized by Imp α through its nuclear localization sequence (NLS). The cargo/Imp α complex binds to Imp β forming an import complex. The import complex is disassembled by RanGTP on the nuclear side. The Imp β/RanGTP complex shuttles back to the cytoplasm directly whereas Imp α requires CAS/RanGTP for recycling. Activation of the RanGTPase and disassembly of the Imp α/CAS/RanGTP and Imp β/RanGTP export complexes minimally requires RanGAP and a Ran binding protein (RanBP). Ran is recycled back to the nucleus by NTF2, whereupon GDP/GTP exchange is promoted by RanGEF. For simplicity, NTF2 is shown as a monomer, although *in vivo* the dimer form is expected to dominate [107].

directly monitoring single molecules diffusing in aqueous solution [21,47]. Imaging rates for single molecule nuclear transport experiments are typically about 200–1000 fps [20,21,48–50]. Important advantages for these experiments are that NPCs are embedded within a well-defined cell structure (the NE) that is easily visualized, that NPCs are essentially immobile in higher eukaryotes due to interactions with the nuclear lamins, and that the spacing between NPCs is typically large enough to be resolved by light microscopy [51]. This implies that individual NPCs can be easily found within a cell, and that multiple molecules can be individually and successively imaged transiting through the same NPC, even if the time between interactions is long relative to the transit event itself. Immobile NPCs are critical for distinguishing multiple discrete events at the same pore and for distinguishing pore movement from the movement of transiting molecules.

Multiple approaches have been used to image single fluorescent molecules interacting with NPCs. Total internal reflection fluorescence (TIRF) microscopy is commonly used in the SMF field. However, this approach typically relies on complete reflection of the excitation beam at a glass–water interface. This approach illuminates molecules at or near the glass surface via an evanescent field, and thus, is unsuitable for detection of molecules deep within a cell. Traditional wide-field epifluorescence microscopy is sensitive enough to detect single fluorescent molecules under the appropriate conditions [52,53], but the background noise level makes it difficult to achieve the sensitivity needed for rapid nuclear transport experiments. However, an improved S/N is obtained with a restricted illumination area. The illumination area can be controlled by a pinhole in the illumination path, as in narrow-field epifluorescence microscopy [50], or via a fiber optic [54]. The S/N can be enhanced even further, by at least 2-fold, when the excitation beam enters the sample at a sub-TIRF angle. This approach has been termed highly inclined and laminated optical sheet (HILO) microscopy [55]. Single-point edge-excitation sub-diffraction (SPEED) microscopy represents the small area limit of the HILO approach. In SPEED microscopy, the excitation beam is focused in the image plane yielding a diffraction-limited focal volume, which is sufficiently large to image individual NPCs and molecules transiting through them [56]. These approaches have been used to obtain the experimental SMF data discussed in this review.

4.1. Nuclear transport in live and permeabilized cells

Nucleocytoplasmic transport has been studied by light microscopy for decades. For real-time experiments, both live and permeabilized cell approaches are used. In both cases, the basic requirements are that the nuclear and cytoplasmic compartments are distinguishable, and the protein of interest must be detectable. The protein of interest is identified by a fluorescent tag. In the case of live cell experiments, fluorescent modification is commonly accomplished with one of the many genetically-encoded fluorescent proteins available [57]. Genetically-encoded fluorescent protein tags are especially useful for yeast cells, which have a tough cell wall that inhibits the introduction of fluorescent molecules by other methods [58]. Unfortunately, yeast NPCs are mobile [59], presenting difficulties for developing single molecule approaches since NPC movement must be distinguished from the movement of molecules passing through. Genetically-

encoded fluorescent proteins are larger in size and less photostable than organic dyes, and hence, organic dyes are preferred for SMF experiments. To date, SMF experiments on nucleocytoplasmic transport have been restricted to mammalian cells. *In vitro* purified and fluorescently tagged proteins can be microinjected and followed at the single molecule level in live cells [21,48]. In principle, these are the ideal experiments since observations are made under native conditions. However, the concentrations of exogeneous and endogeneous transport factors are not easily controlled and determined, and thus, an *in vitro*/in organello approach is preferable for many SMF experiments. Permeabilized mammalian cells are obtained by treatment with a low concentration of the detergent digitonin. The nuclear envelope remains intact, and nucleocytoplasmic transport can be reconstituted with cell extract [60]. Since many protein factors required for nucleocytoplasmic transport have been identified and isolated, *in vitro* transport assays using purified components and digitonin-permeabilized cells are well established (for example, see [38,61–64]). SMF experiments have retained all the conditions of the basic permeabilized cell assay, simply reducing the fluorescent molecule of interest to a dilute concentration level suitable for single molecule imaging [20,49]. An *in vitro* mRNA export assay has been developed [65], but no SMF experiments making use of this assay has been reported. However, a single molecule mRNA export assay in live mammalian cells has recently been reported [66]. Nonetheless, single molecule nuclear transport experiments have thus far concentrated on nuclear import rather than export, primarily due to technical simplicity.

4.2. Locating single molecules

Unless a super-resolution image acquisition method is used (e.g., 4Pi, I^5M, structured illumination, or STED microscopy [67]), individual fluorescent molecules are detected as diffraction-limited spots under the light microscope [53]. The fluorescent intensity follows an approximately Gaussian distribution around the molecule's center location with a width determined by the wavelength (a typical width is 0.2–0.3 μm in the focal plane for a numerical aperture of 1.4 or higher), which is called the point spread function. Thus, the 'apparent' size of the molecule is typically approximately two orders of magnitude larger than the fluorophore itself. Logically, the actual position of the molecule is at the center of the detectable fluorescence intensity distribution. Using an optimized system, single fluorescent molecules can be located with ~1 nm precision [68]. Normally, the accuracy is assumed to be a similar value. The main variables contributing to the precision of this approach are the background noise and the total number of photons collected. Both of these variables are difficult to maximize for single molecule measurements of nuclear transport due to the complex environment and the rapid Brownian movement of the fluorescent particles, which necessitates short integration times. The background noise is dependent both on intrinsic noise (contributions from the imaging system and the sample environment) and extrinsic noise introduced by the experimental procedures (e.g., out-of-focus diffusing fluorescent particles identical to the one being imaged). The movement of diffusing particles limits the precision with which the particle can be located during the image acquisition period. Hence, for a dynamic system, shorter integration times should lead to better localization precision. However, a shorter integration time implies fewer photons collected in each frame, and hence worse precision, unless the emission intensity can be correspondingly increased. Thus, high spatial resolution measurements for diffusing particles require both high excitation intensities and high frame rates. Most SMF experiments of molecules transiting NPCs have an accuracy of ~40–50 nm [50]. The SPEED approach yields 0.4 ms time resolution and 10 nm static spatial precision [56], yielding an accuracy of ~20 nm for mobile particles [50]. 4Pi microscopy also provides ~10 nm static spatial resolution, but does not yet have single molecule sensitivity [69]. A static precision of 6 nm has been obtained with nuclear-targeted quantum dots [70]. The utility of quantum dots as a general label for nuclear transport experiments is unclear, however, due to the lower time resolution (40 fps) of the study and the large size of the coated quantum dots (~18 nm) [70], which likely significantly perturbs the behavior of molecules passing through a 45–50 nm pore.

The lesson from the last paragraph is that the errors for the majority of single molecule position measurements in nuclear transport experiments to date are relatively large, especially compared to current state-of-the art measurements in other fields such as motor proteins [71]. Thus, one should not assign too much importance to any individual particle trajectory point, especially without knowing the S/N (precision) for that particular imaging frame. However, single molecules can clearly be detected interacting with NPCs, and sometimes passing through (Fig. 2). An average of many measurements can certainly provide important biological information and be significantly more precise than a single measurement. For example, Fig. 3 shows the distribution of CAS position measurements. The data indicate that, while in the NPC, CAS spends the majority of the time on the nucleoplasmic side of the pore. This approach has been used to estimate the average position along the *z*-axis (transport axis) for numerous proteins and nuclear transport cofactors (Fig. 4 and Table 1). For these position measurements to be meaningful, a point of reference is necessary. Relative distances between various points of reference are shown in Fig. 4. Notably, most of the tested molecules spend most of their pore residence time interacting with central regions of the NPC – CAS is a notable exception. In this review, all points of reference are to the NE, as determined from a bright-field image.

4.3. Interaction times and transport efficiencies

The simplest primary piece of information obtained from single molecule nuclear transport measurements is the fluorescent particle's interaction time (also called residence time or dwell time) at the pore. The interaction time is a measure of how long the particle spends interacting with nuclear pore proteins. Reported interaction times for typical protein cargos range from ~33 ms to <1 ms, depending on conditions and the particular molecule, with most proteins having interaction times of 5–10 ms (Fig. 5 and Table 2). These values are obtained by fitting a single exponential decay to a frequency histogram of individual particle interaction times (Fig. 2C). Minor populations (up to 10%) of some proteins have significantly longer interaction times [48], though it is not clear what such data indicate. Single exponential fits to interaction time histograms suggest that there is a single rate-limiting step in the transport reaction, e.g., binding to RanGTP or escape from the pore. For particles transiting through the NPC, there are certainly many translocation substeps in order for the particle to migrate across a ≥~50 nm thick permeability barrier. A series of multiple slow rate-limiting substeps would produce a delay in the appearance of the transported molecules, which has not been observed for proteins. For proteins, therefore, substeps must occur rapidly, relative to the total interaction time. In contrast, β-actin mRNA has a noticeably longer NPC interaction time (~180 ms), requiring at least two slow rate-limiting steps. Interesting, mRNA transport through the pore is relatively fast (5–20 ms), but docking and release on the nucleoplasmic and cytoplasmic sides of the pore, respectively, are slow (~80 ms each) [66], presumably due to mRNA processing and association/dissociation events that must occur in these locations [72].

Not all molecules that interact with the FG-network end up crossing the permeability barrier. To explicitly demonstrate this fact, a given molecule must be visualized before it interacts with an NPC as well as after it leaves that NPC (Fig. 2). Under normal transport conditions in permeabilized cells with 2 ms time resolution, about

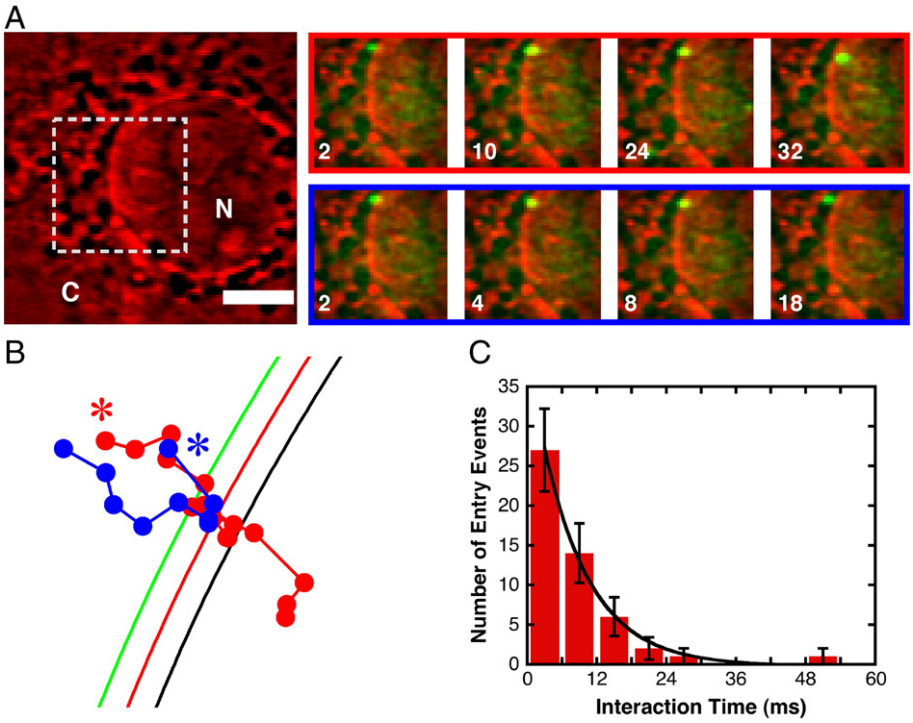

Fig. 2. SMF imaging of nucleocytoplasmic transport. (A) Select video frames demonstrating an import event (*top*) and an aborted import event (*bottom*) in a permeabilized HeLa cell. Both fluorescent cargo molecules (NLS-2xGFP) interacted with the same NPC. The large, bright-field image on the left shows the nucleus (N) and the cytoplasm (C). The smaller images, corresponding to the boxed region in the large image (same scale), are 2 ms video frames consisting of SMF signals (*green*) overlaid onto a bright-field image (*red*) obtained with the same camera. Numbers correspond to time in milliseconds. Bar: 5 μm. (B) Trajectories for the two interaction events shown in (A) with all frames included: (*red*) entry event; (*blue*) abortive event. The beginning of each trajectory is identified by a star (*). The red curve is the experimentally determined position of the NE from the bright-field image; the green and black curves are for reference at −100 nm and +100 nm from the NE, respectively. (C) Histogram of interaction times for cargos that entered the nucleus ($\tau = 8.0 \pm 0.4$ ms, $N = 51$). For comparison, a histogram of interaction times for cargos that underwent abortive transport yields $\tau = 8.6 \pm 0.7$ ms, $N = 49$ (not shown). ©Yang & Musser, 2006. Figs. and captions originally published in *The Journal of Cell Biology*. doi: 10.1083/jcb.200605053.

$1/6^{th}$ of the observed NPC interaction events fall into this category [21]. The limitation is that the fluorescent molecule of interest must remain within the focal plane for at least one image frame before and after its NPC interaction. Most of the time, the molecule diffuses out of the focal plane too quickly. Higher time resolution is expected to increase the number of useful transport trajectories, but until rapid 3D imaging is possible, there will always be some trajectories that must be discarded. Note that a trajectory discarded from transport efficiency calculations is still useful for interaction time measurements, if it is assumed that the disappearance of a fluorescent spot is not due to photobleaching.

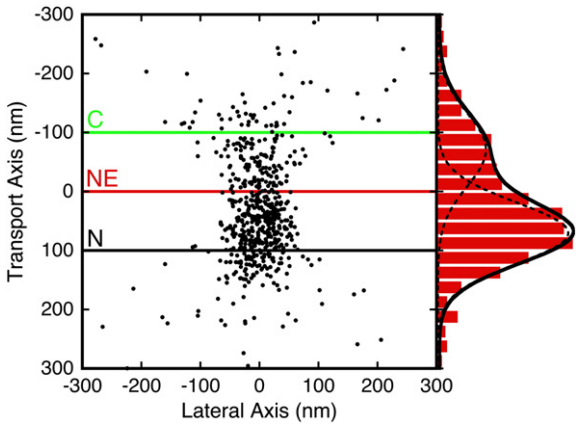

Fig. 3. Distribution of CAS within the NPC. Shown here are CAS positions detected in the presence of Imp α, Imp β, Ran, NTF2 and GTP. Included in the histogram analysis are all data within ± ~1 μm of the NPC center. However, only central positions are shown. A positive number along the transport axis reflects the nuclear side, i.e., the nucleoplasm (N) is at the bottom of the figure and the cytoplasm (C) is on the top. The two Gaussian fits to the histogram yield 70 ± 52 nm (69%) and -71 ± 63 nm (31%) ($\mu \pm \sigma$). Data is from Fig. 3C of Sun et al. [40].

Transport efficiencies of the NLS-2xGFP cargo under relatively low Imp β concentrations (up to ~0.5 μM) are ~50% [21]. In principle, molecules that abort transport and molecules that complete full translocation through the NPC could have different interaction times. One possibility is that molecules that only partially penetrate the permeability barrier (e.g., due to jamming of the channel), or those that encounter only the cytoplasmic periphery of the NPC can more easily abort transport, leading to a shorter interaction time for abortive molecules [73]. On the other hand, for the Imp β1 pathway, binding of RanGTP to the transport complex promotes cargo release from the NPC [20,74]. Since the RanGTP concentration is higher in the nucleoplasm than in the cytoplasm, cargo molecules that abort transport most likely must reach the nucleoplasmic side of the pore and then return back to the cytoplasm. This picture is supported by single molecule experiments, which demonstrate that the Imp α/cargo interaction is preferentially broken in the nuclear basket region and that the free Imp α and cargo molecules can enter the nucleus or return to the cytoplasm [40]. This picture also predicts longer interaction times for abortive transport, since cargos that abort transport must migrate a longer distance (to nucleoplasmic side and back) before release from the NPC. Current interaction time data is inconclusive on this point — in most, but not all, cases, the difference between abortive and actual transport interaction times is statistically insignificant. However, the mean time constants for abortive transport are consistently 0.2–0.6 ms longer than for actual transport [21], suggesting that higher resolution data would statistically support the second model. This discussion suggests caution when comparing interaction times. Most interaction times are assumed, or interpreted, to represent actual transport times. In most cases, this assumption is probably valid within the experiment's time resolution.

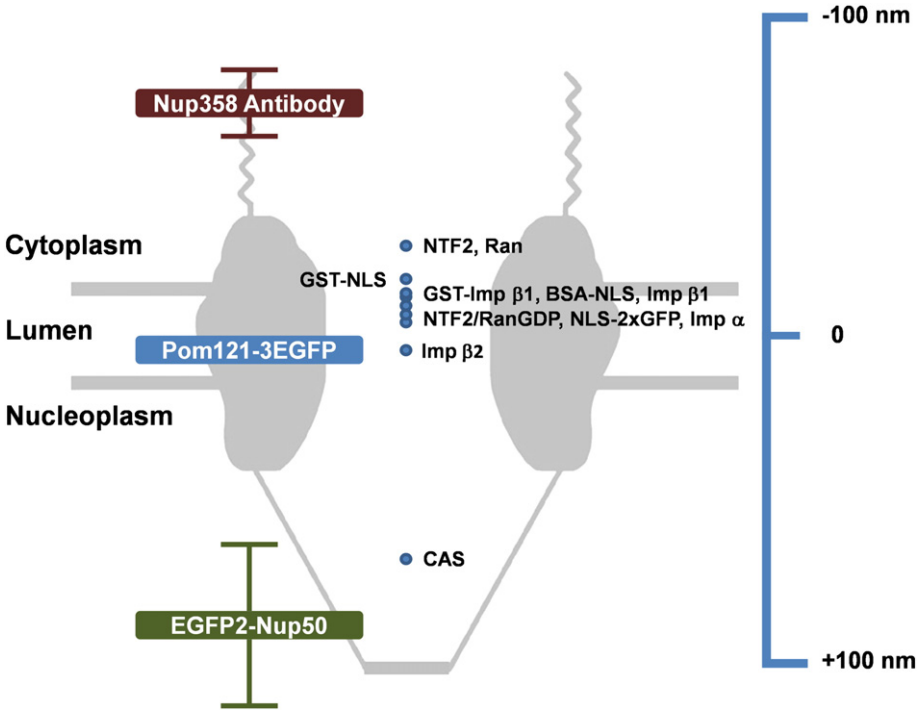

Fig. 4. Most probable positions of selected NPC proteins, transport cofactors and cargos within the NPC. The NE position determined from bright-field imaging is set to 0 nm along the transport axis. NPC reference points are provided on the left. In general, transport cofactors and cargos have wide, not always symmetrical, distributions within the NPC. Note that no differentiation is made between multiple oligomeric complexes that are possible. Details are provided in Table 1.

However, one must be careful in reading too much into small differences in interaction times since abortive and actual transport times are not reported in many cases, and there are theoretical reasons to believe that small differences could exist.

It has been estimated that the diffusion constant, D, within the NPC for the NLS-2xGFP cargo is ~1 $\mu m^2/s$, or about 10-fold less than that in the cytoplasm. This is considered to represent a minimum estimate for D since the measurements reflect movement in a confined space [21], and thus, large displacements are not possible. Considering this value for D, an 8–9 ms interaction time [21] implies that the molecule can cross the permeability barrier ~6–7 times ($r^2 = 2Dt$, where $r \approx 50$ nm) before exiting the pore (or ~3–4 times back and forth). This is consistent with the earlier discussion, in which it was concluded that the transport substeps are fast relative to the rate-limiting exit step. At high Imp β1 concentrations, the NLS-2xGFP interaction time decreases to ~1 ms, suggesting that time exists for only ~1 transit across the permeability barrier. It is under these conditions where a statistical significance between abortive and actual transport times was observed [21], supporting the interpretation that abortive molecules cross the permeability barrier at least twice before release. However, due to

Table 1
Most probable locations of NPC proteins and transport cofactors.

Reference	Fluorescent molecule	Most probable position[a] (nm)	Permeabilized or live cells	Source
NPC proteins				
Bright-field NE	EGFP2-mNup50	92 ± 33	*in vitro*	[40]
Bright-field NE	rPom121-3EGFP	15 ± 5	*in vitro*	[21]
Pom121-GFP	Nup358 Antibody	−72 ± 75	*in vitro*	[49]
Transport cofactors				
Bright-field NE	CAS[b]	70 ± 61	*in vitro*	[40]
Pom121-GFP	Transportin (Imp β2)	5 ± 75	*in vivo*	[48]
Pom121-GFP	Imp α[c]	−6 ± 80	*in vivo*	[48]
Pom121-GFP	Alexa633-Ran (with NTF2)	−9 ± 38	*in vitro*	[69]
Pom121-GFP	Imp β1	−10 ± 80	*in vivo*	[48]
Pom121-GFP	GST-Imp β1	−14 ± 26	*in vitro*	[69]
Pom121-GFP	Alexa633-Ran	−30 ± 40	*in vitro*	[69]
Pom121-GFP	NTF2	−30 ± 63	*in vitro*	[49]
Cargos				
Bright-field NE	NLS-2xGFP[c]	0 ± 59	*in vitro*	[20]
Pom121-GFP	BSA-NLS[c]	−13 ± 70	*in vivo*	[48]
Pom121-GFP	GST-NLS[c]	−17 ± 24	*in vitro*	[69]

[a] Positions relative to the bright field image of the NE with the positive direction towards the nucleus. Position determinations typically yield wide distributions. To reflect the broad localizations, values are reported as mean ± 1/2 FWHM (full width at half maximum). FWHM values are reported values or best estimates. For a Gaussian distribution, FWHM = 2.35σ.

[b] See Fig. 3 for more details on binding conditions and distribution.

[c] Imp β and Imp α (if necessary) were included in the assay to mediate NPC binding.

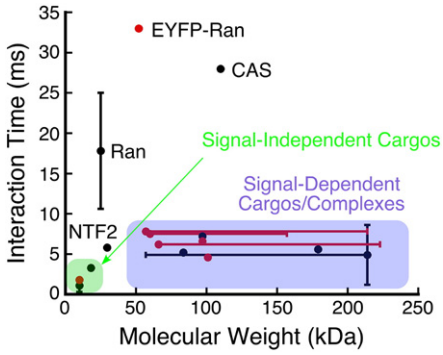

Fig. 5. Interaction times of various transport cofactors and cargos with the NPC. Data come from Table 2. For the *in vitro* data (*black*), molecular size is more reliably estimated since the major species can be controlled by experimental conditions. However, it should be remembered that transport complexes do not always remain the same size during transport, e.g., the Imp β/Imp α/cargo complex disassembles during cargo import. For the *in vivo* data (*red*), molecular weights represent the minimum expected. Horizontal bars indicate the expected range in molecular weight during transport. Complexes and cofactors of signal-dependent protein transport pathways typically have interaction times of 5–10 ms (*purple region*), regardless of molecular weight. The smaller signal independent cargos have interaction times<5 ms (*green region*). Transport cofactors can have lengthy interaction times, consistent with their functional roles at the NPC itself. In some cases, different environment conditions result in a range of interaction times, as indicated by vertical bars. Not shown is the interaction time of ~180 ms for actin mRNA particles (~4–5 MDa), of which only ~5–20 ms is spent migrating through the NPC [66].

insufficient time resolution, it is not known whether the diffusion constant within the NPC changes under these conditions. It is reasonable to assume that the diffusion constant does change, but if so, probably not enough to completely compensate for the decrease in interaction time. This may explain why the difference between abortive and actual transport events becomes distinguishable at high Imp β1 concentrations. Higher time resolution measurements are expected to help settle this issue. Importantly, the thickness of the permeability barrier (the range of the FG-Nup network) is crucial for understanding these data, and remains to be resolved to high precision.

Table 2
Interaction Times of cargos and transport cofactors with NPCs.

Fluorescent molecule	Interaction time (ms)	Permeabilized or live cells	MW (kDa)	Source
Transport cofactors				
NTF2 (dimer)	5.8 ± 0.2	*in vitro*	30	[49]
NTF2/RanGDP (dimer)	5.2 ± 0.2	*in vitro*	84	[49]
Transportin (Imp β2)	7.2 ± 0.3	*in vitro*	97	[49]
Transportin (Imp β2)	4.6 ± 0.1	*in vivo*	97[a]	[48]
Transportin/M3-GST	5.6 ± 0.2	*in vitro*	179	[49]
Imp α	7.5 ± 0.8	*in vivo*	60[a]	[48]
Imp β1	6.6 ± 0.2	*in vivo*	95[a]	[48]
CAS	28 ± 1	*in vitro*	110[a]	[40]
EYFP-Ran	33 ± 14	*in vivo*	52[a]	[92]
Ran	10–25[d]	*in vitro*	25[a]	[69]
Protein cargos (signal-dependent import)				
BSA-NLS	6.2 ± 0.3	*in vivo*	68[a]	[48]
NLS-2xGFP	1.0–8.8[d]	*in vitro*	58[a]	[21]
NLS-2xGFP	7.8 ± 0.4	*in vivo*	58[a]	[21]
Nucleic acid cargo (signal-dependent export)				
Actin mRNA	180 ± 10[b]	*in vivo*	1100[c]	[66]
Cargos (signal-independent)				
Dextran	1.8 ± 0.1	*in vivo*	10	[21]
Dextran	<0.5–2.2[d]	*in vitro*	10	[21]
rpS13	3.3 ± 0.1	*in vitro*	18	[21]

[a] Identified is the molecular weight (MW) of the cargo or transport cofactor. For most *in vivo* and some *in vitro* experiments, MWs are not well-defined since the oligomerization state and/or cargo is unknown. In addition, note that the MW may change during transport due to association/dissociation events.

[b] The time required to transport through the pore is ~5–20 ms. The majority of the interaction time is spent docked on the nucleoplasmic (~80 ms) and cytoplasmic (~80 ms) sides of the pore.

[c] The actin mRNA is 3.3 kb (~1.1 MDa). The total mass of the visualized mRNA export complex is estimated as ~4–5 MDa.

[d] Different interaction times were obtained under different conditions.

4.3.1. Simple diffusion model

It is instructive to examine the predictions of a simple diffusion model. A good place to start is with the diffusion model of Frey and Görlich [17]. Similar derivations, albeit with different nomenclature, are provided by Zilman and coworkers [75,76]. The basic model is shown in Fig. 6A, where it is assumed that a transiting molecule has concentrations C_C and C_N in the cytoplasmic and nucleoplasmic compartments, respectively. For a transport pathway like the Imp β1 system in which nuclear rimming is observed, the NPC clearly provides an attractive potential of energy $-u$ (Fig. 6B). Thus, the concentration at the cytoplasmic interface, C_{BC}, is expected to be higher than C_C. Similarly, the concentration at the nucleoplasmic interface, C_{BN}, is expected to be higher than C_N. Under equilibrium conditions, the ratio of the concentrations on both sides of the cytoplasmic and nucleoplasmic interfaces defines a partition coefficient [17]:

$$e^u = K = \frac{C_{BC}^{eq}}{C_C^{eq}} = \frac{C_{BN}^{eq}}{C_N^{eq}} = \frac{k_1}{k_{-1}} \quad (1)$$

where u is assumed to be in units of RT. In this model, the partition coefficients on both sides of the NPC are identical. This follows from the square potential well outlined in Fig. 6B. Under non-equilibrium conditions, a concentration gradient drives net translocation through the NPC, and thus, C_{BC} and C_{BN} cannot be determined from Eq. 1. However, the rate constants for particle movement into and out of the barrier, k_1 and k_{-1}, do not change (at least, they are not expected to).

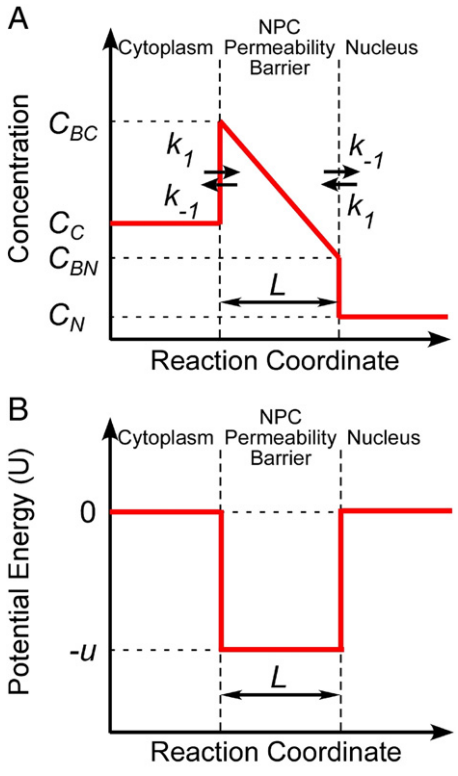

Fig. 6. Simple Diffusion Model of transport across a permeability barrier. Net transport occurs from left to right when $C_C > C_N$. The equilibrium partition coefficient, $K = k_1/k_{-1}$, is assumed to be the same on both sides of the barrier. Adapted from Frey and Görlich [17]. See text for details.

In this model, the total flux, J, is [17]:

$$J = \frac{ADk_1(C_C - C_N)}{Lk_{-1} + 2D} = \frac{Ak_1(C_C - C_N)}{2(\gamma + 1)} \quad (2)$$

where we have defined $\gamma = Lk_{-1}/2D$. The variable γ compares the spontaneous exit speed to the average speed of diffusional motion through the pore. Thus, a low γ implies multiple barrier crossings before exit. According to the hydrogel results of Frey and Görlich [17,27], γ is typically less than 0.05 for facilitated transport. Under these conditions, $C_{BC}/C_{BN} \approx 1$ (see Supplemental Information). This model therefore predicts that the transiting species should be approximately homogeneously distributed within the pore, and the total flux can be approximated from Eq. 2 as:

$$J \approx \frac{Ak_1}{2}(C_C - C_N) \quad (3)$$

Yang and Musser [21] defined transport efficiency, E, as the number of particles that exit into the nucleus divided by the total number of particles that enter the pore from the cytoplasm. According to the simple diffusion model described in this section:

$$E = \frac{1}{2(\gamma + 1)} \quad (4)$$

(see Supplemental Information for derivation). This equation indicates that the maximum transport efficiency is 0.5. As mentioned earlier, γ is typically less than 0.05 for facilitated transport through NPCs [17,27]. Thus, this model predicts nuclear transport efficiencies of ~50%.

The definition of transport efficiency provided in the previous paragraph is presumed to be exactly that which is measured in and reported for single molecule experiments. Experimentally, the only molecules that are counted are those that enter the pore, defined by those that have a measureable interaction time [21,40]. Not counted are those molecules that impinge on the pore, but do not actually enter the FG-network. This distinction is important due to semantic differences in the literature. 'Transport efficiency' as defined here is termed 'translocation probability' by Zilman and coworkers [75,77]. These authors include in 'transport efficiency' those molecules that impinge on the pore but do not enter it [75,77]. When the translocation channel is essentially empty, 'transport efficiency' = 'translocation probability'. In crowded channels, some impinging molecules will be rejected by the channel, resulting in 'transport efficiency' < 'translocation probability' [75].

4.3.2. Multi-species diffusion models

The most striking conclusion from the Simple Diffusion Model outlined in the last section is that the transport efficiency can never be greater than 50%. This makes intuitive sense since, in the context of this model, C_{BC} is always expected to be larger than C_{BN} when $C_C > C_N$. However, transport efficiencies greater than 50% have been reported [21]. How can this be? One way that this can happen is if the transiting species has an altered affinity for the pore on the nuclear basket side. For example, the assumption implicit in the Simple Diffusion Model is that the molecular species transiting through the NPC does not change its molecular properties in any way during the translocation process. For the Imp β/Imp α transport pathway, this assumption is invalid. RanGTP is required for release of cargo from the Imp β/Imp α/cargo complex. There are two control points: 1) the binding of RanGTP to Imp β weakens the Imp β/Imp α interaction, leading to dissociation [74,78] – at this point, the Imp α/cargo complex may exit the NPC; and 2) the binding of CAS/RanGTP to Imp α weakens the cargo/Imp α interaction, leading to dissociation – Nup50 promotes this reaction at the end of, or during, transport through the NPC [39–42,79]. The first reaction is expected to be largely quantitative, i.e., this reaction is essential for cargo to escape from the NPC, since in the absence of RanGTP, Imp β/Imp α/cargo complexes remain tightly bound to the NPC for long periods ("nuclear rimming") [20,74]. Single molecule fluorescence resonance energy transfer (smFRET) experiments indicate that the second reaction is not quantitative, at least *in vitro*, since some Imp α/cargo complexes escape from the NPC intact [40].

The disassembly of Imp β/Imp α/cargo complexes during transport complicates the concentration gradient picture. In fact, the smFRET experiments of Sun and coworkers [40] indicate that there exist non-zero cargo and Imp α/cargo complex concentrations within the NPC. These data indicate that Imp α/cargo complexes can dissociate during transit through the NPC, and that sometimes the free cargo returns to the cytoplasm. The data further suggest that the dissociation event occurs near the nuclear exit interface. Therefore, when a free cargo molecule generated by dissociation of an Imp α/cargo complex near the nuclear exit interface returns to the cytoplasm, the free cargo must diffuse back through the channel. Similarly, the same experiments showed that intact Imp α/cargo complexes can return back to the cytoplasm [40]. RanGTP is required to dissociate Imp β from Imp β/Imp α/cargo complexes, and the expectation is that encounters with RanGTP occur predominantly near the nuclear exit interface due to the steep RanGTP gradient across the NE [45]. This argument therefore predicts that free Imp α/cargo complexes also likely can diffuse back through the channel. In this model, Imp α/cargo complexes are expected to be more prevalent near the nucleoplasmic exit site (see Fig. 7), and thus, they should be preferentially released into the nucleoplasm, as indeed they are [40]. Free cargo molecules are also preferentially released into the nucleoplasm [40], supporting a free cargo distribution similar to that shown for Imp α/cargo complexes in Fig. 7. Competition for space likely alters these concentration profiles from a simple linear picture [77]. The lesson here is that import efficiencies near 1 are easily understood if the transiting species undergoes changes in molecular structure during transport.

4.3.3. More sophisticated models

Since signal-independent cargos do not require RanGTP and do not change in molecular structure during transport, one might expect that the Simple Diffusion Model is an appropriate model for these cargos. However, the import efficiency of 10 kDa dextran increased from ~50% in the absence of Imp β to ~67% in the presence of 0.5 μM Imp β [21]. Thus, dextran transport efficiencies are not explained by the Simple Diffusion Model. The 10 kDa dextran cargo is assumed to be an inert, signal-independent cargo that does not bind to elements of the nuclear transport system, and its small size presumably allows it to diffuse through the NPC without binding to any NTRs. Perhaps the inertness assumption is invalid and dextran binds weakly to Imp β and/or elements of the NPC. However, exogeneous RanGTP was absent from the dextran experiments, and thus was not available to

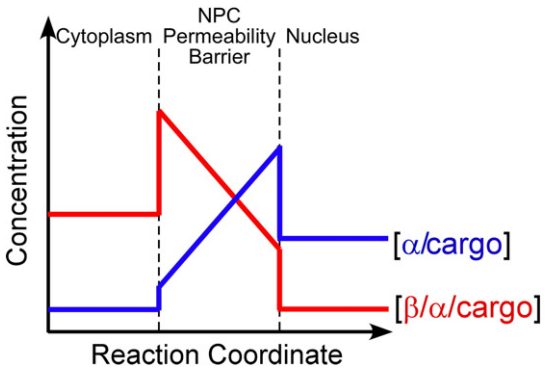

Fig. 7. Differential concentration gradients for different species. Association and dissociation events can dramatically affect concentration gradients. See text for details.

modulate potential weak interactions. A counterargument is that the endogeneous RanGTP retained in permeabilized cells [40] may be sufficient to explain the observed results. An alternate possibility is that the Simple Diffusion Model is too simple even for signal-independent cargos, and that a more complex model is required for these cargos.

The flux models discussed in the previous sections provide a simple overview of particle movement though pores, yet they are highly idealized and constrained. More complex models are required to accommodate more realistic conditions or more complex questions. For example, the potential energy surface within the pore is not expected to be flat, due to the inhomogeneity of the FG-network. Further, it would be useful to predict transport times as well as to determine the effects of interaction strength and high local concentrations ('jamming' of the pore) on transport times and efficiencies. Using a more complex analysis based on the basic diffusion picture and Monte Carlo simulations, Zilman and coworkers [75–77] found that, in the absence of jamming, the pore's transport properties were relatively insensitive to the shape of the potential energy surface and whether the potential surface was represented by multiple wells (many binding sites) or a single well. A favorable interaction energy is clearly required to access the FG-network. Very high interaction strengths lengthen transport times due to highly favorable interactions with the FG-network, but can also promote transport efficiencies near 100%. These high transport efficiencies require RanGTP to modulate affinity for the FG-network, as discussed earlier. Under optimal transport efficiency conditions, a particle within the pore is inhibited from going backwards since a second incoming particle inhibits backwards movement. At lower concentrations, the first particle can return to the cytoplasm before a second binds, reducing transport efficiency. At higher concentrations, particles already within the pore reject incoming particles, also reducing transport efficiency. The jamming transition occurs at the point of maximum transport efficiency, which occurs when about half the sites within the channel are occupied [75]. Note that the transport efficiency discussed here is the Zilman definition of transport efficiency, not the Zilman translocation probability, which corresponds to E as defined earlier. As discussed previously, the Zilman translocation probability is presumably what is measured in single molecule transport experiments, and it is unclear if the Zilman transport efficiency can be measured directly.

The Zilman model also predicts that the presence of a strongly interacting species dramatically reduces the possibility for a weakly interacting species to penetrate the barrier [76,77]. This prediction has been confirmed experimentally with intact NPCs, FG hydrogels, and in artificial nanopores decorated with FG-containing polypeptide fragments [27,80,81]. In the aforementioned 10 kDa dextran experiments, the cargo concentration was so low that cargo jamming cannot be invoked to explain the high transport efficiencies observed in the presence of high Imp β concentrations. Further, dextran is a weakly interacting species and the Zilman model predicts lower, not higher, transport efficiencies in the presence of a strongly interacting species, such as Imp β [76]. So, the dextran transport efficiency data remain unexplained.

The NPC promotes bidirectional transport, i.e., both import and export. The pore is large enough so that it seems safe to assume that both of these processes continue simultaneously. When a very large cargo similar in size to the diameter of the pore is being transported, such as a ribosomal subunit or a virus [82,83], it is logical to expect that the import and export of other cargos would be partially or completely inhibited. It was earlier noted that import efficiencies can be modulated due to jamming. Jamming can promote import while simultaneously inhibiting export. These jamming effects can be quite strong since import complex dissociation factors (e.g., Nup50, CAS, and RanGTP) are found mostly near the nucleoplasmic face of the pore. Thus, import complexes may accumulate on the nucleoplasmic side, inhibiting the entry of export complexes. Kapon et al. [84] modeled this and found that the NPC can fluctuate between an importer (import dominates) and an exporter (export dominates). Part of this is simply due to stochastic fluctuations. However, they found that the jamming and the localization of dissociation factors allows the NPC to persist in the importer and exporter states longer than simple stochastic fluctuations predict. Further, since the direction of net movement that dominates is determined by concentration, the transport activity most needed dominates. This modulation of transport activity does not require any additional information sensing pathways, and thus allows the cell to very simply adjust traffic in response to cellular demands [84]. In these simulations [84], it was assumed that the transiting species had some degree of preference to travel in a specific direction. Biased diffusion has not been observed in single molecule experiments [20]. Rather, at least for signal-dependent cargos, biased release from the pore seems to arise from the interactions with Ran, which implies that the transiting species changes during transport. This was not explicitly modeled by Kapon et al. [84].

4.4. Properties of and changes in the permeability barrier

A major barrier to comprehending the selectivity and transport properties of the NPC is our incomplete understanding of the structural and functional properties of the FG-network. The basic conceptual issues are the following. The FG-Nups each contain a globular anchor domain, which is embedded in or attached to the framework of the NPC. The remaining portion of each FG-Nup contains a series of FG repeat motifs separated by short (~10–20 amino acid residues), largely hydrophilic segments [15,85]. The FG-domains do not form recognizable secondary structure, but rather are deemed intrinsically, or natively, unfolded [86]. Thus, the FG-domains are essentially polymeric strings tethered to the NPC scaffold. In good solvents, tethered polymers will adopt one of two configurations, a mushroom structure at large spacings and a brush structure at small spacings. In poor solvents, both structures will collapse [87,88]. These are the basic physical properties of polymer arrays. However, there are additional levels of complexity. The FG-polymers are too long to be accommodated in a fully extended configuration on the cylindrical walls of the central pore of the NPC without clashing in the middle [18,86]. Formation of a brush structure certainly helps since the polymer chains would no longer be fully extended [18,86], but the space available to the tips of the polymers (center of the pore) is less than that available to the tethered ends (periphery of the pore). It is unclear how these geometrical constraints affect polymer behavior. One solution is that different FG sub-domains adopt different structures, some of which are relatively compact, thereby allowing for efficient packing within the cylindrical pore [85]. The inhomogeneity of the polypeptides themselves, the hydrophobic FG repeats interdispersed within otherwise hydrophilic polymers, presents solubility problems. Consequently, the FG-polymers are difficult to work with in isolated form and are prone to aggregation, except under pH extremes, with denaturants [17,89], or as fusion proteins [86]. Aggregation in water implies strong interactions, typically due to the "hydrophobic force" (hydrophobic collapse). Görlich and coworkers have proposed that the FG repeats interact to yield a hydrogel structure, satisfying the hydrophophic interactions while simultaneous keeping the polypeptides soluble and infiltrated with aqueous solvent. FG-domains do not require the NPC anchor domains to form stable hydrogels [17,27,89], suggesting that the hydrogel structure is an inherent property of the polypeptides rather than a structure dictated by the precise geometric arrangement in the NPC. An additional intra-FG-polypeptide structural motif was recently discovered. Asn-rich spacer regions form kinetically stable amyloid-like β sheets, resulting in a tough hydrogel [90]. Thus, at least some FG-polymers are not inert, and intrachain interactions likely cause

significant deviations from strict, non-interacting polymer physics behavior. In addition, the net positive charges in the FG-domains are expected to lower the energy requirement for negatively-charged transport receptors to enter the barrier [7]. Gel behavior does not require strong interactions between the polymers — many weak interactions would suffice [87]. A variety of different interchain affinities could certainly lead to a glass-like transition rather than sharp gelation behavior [87].

The general assumption thus far is that the permeability barrier is determined largely or entirely by the inherent properties of the FG-network — the key phrase being 'inherent properties'. However, it is not clear that this is true. As mentioned earlier, it has been shown in both intact NPCs and in model systems that the permeability barrier is more selective in the presence of Imp β than in its absence [27,76,80,81]. One interpretation is that this is simply a result of jamming the channel. However, it is also possible that the presence of Imp β fundamentally alters the properties of the permeability barrier. Single molecule experiments suggest that this is indeed the case. In the presence of 0.5 μM Imp β, the 10 kDa dextran import efficiency increases from ~50% to ~67% and the transport time is cut in half, from ~2 ms to ~1 ms, compared to the absence of Imp β [21]. These are not the expected effects for a jammed channel, according to current models [75,76]. Due to changes in the import efficiency and transport time of NLS-2xGFP by 5 μM Imp β, the V_{max} for transport of this signal-dependent cargo is estimated to increase by ~10-fold [21]. Again, this is not the expected result for a jammed channel. However, it is indeed possible that high Imp β concentrations enable an increased accessibility to RanGTP, and that this alone explains the results for signal-dependent cargos. But RanGTP accessibility does not appear to explain the dextran data since exogeneous Ran was not present in those experiments.

The central pore of a yeast NPC has a volume of ~30,000 nm^3 [17]. If all the FG-repeats (~5.27 MDa) [91] are packed into this central pore, they would occupy about 6500 nm^3, or ~20% of the available space. A single vertebrate NPC can simultaneous accommodate at least ~100 Imp β molecules, about half that number of Imp α molecules, and 50–200 Ran molecules [55,92,93], which together would occupy close to ~20% of the central pore volume. Thus, the protein component of the permeability barrier within NPCs *in vivo* is about half transport cofactors and about half FG-polymers. At this loading, or occupancy, of the FG-network, it is not unexpected that the permeability barrier has altered properties [94]. Imp β has five experimentally verified FG binding sites and five additional predicted FG binding sites [95–99]. Thus, Imp β itself can act as tiny droplets of glue that hold the FG-network together. If all the FG-repeats and the transport cofactors mentioned above are found in the central pore, the protein concentration in this region would be over 500 mg/mL. This is quite high. For comparison, the protein concentration within the cytoplasm is typically around 200–300 mg/mL [100]. Based on abortive transport events in single molecule experiments, it seems more likely that the FG-repeats extend beyond the central pore, and, in vertebrates, form a cloud that extends at least 100 nm along the transport axis [21,40]. If this is indeed the case, the protein concentration in the FG-network cloud would be more closely matched to the cytoplasmic protein concentration.

5. Conclusions and prospects

The FG-network is the crucial component controlling transport through NPCs. Single molecule experiments have provided a number of important insights concerning the properties of this material. First, the behavior of molecules interacting with NPCs does not reveal directional movement. Rather, movement within the FG-network appears to be unbiased Brownian diffusion [20]. Second, molecules that interact with NPCs do not always transit through them [21]. This is a necessary consequence of the random movement within the FG-network — backwards movement leads to aborted transport. As far as we are aware, the NPC is the first membrane pore system for which aborted transport has been directly imaged. Third, while movement itself within the NPC may be unbiased, the FG-network does appear to contain a variety of different nanoenvironments that can potentially introduce biases. For example, CAS preferentially interacts with the nucleocytoplasmic side of the pore, Imp α/cargo complexes are preferentially dissociated on the nucleoplasmic side of the NPC [40], and two recent studies suggest that Imp β preferentially interacts with the peripheral regions of the pore rather than the pore center [56,101]. Future studies are likely to reveal more nanoenvironments. Fourth, transport efficiency depends upon conditions. This may result from perturbations to the FG-network structure itself, changes in various nanoenvironments or affinities, loading of the pore, or some combination of these possibilities. Theoretical models will be crucial for distilling the NPC's variable permeabilities as a consequence of various occupancy states.

Single molecule techniques have clearly proven useful for understanding various aspects of nucleocytoplasmic transport. Current technologies are certainly suitable for a wide range of experiments on different transport pathways and cargos. Nonetheless, numerous imaging improvements are both desired and feasible. First, the S/N is always an issue for SMF experiments. Current solutions, such as the HILO and SPEED approaches [55,56], indicate that the S/N is improved by smaller illumination areas and off-axis illumination. Time resolution is also increased with smaller image areas. Sub-millisecond imaging is feasible [56], minimizing the localization errors due to diffusion. The trade-off, however, is context — it is difficult to decipher exactly what is being imaged if the image is tiny. One solution is to combine rapid confocal imaging with SMF imaging. Second, SMF nuclear transport studies have thus far been restricted to two spatial dimensions. A better picture is expected with 4D particle tracking (3D in space plus time). Numerous solutions exist [102–105], but the range of the third dimension in a particular experiment will likely dictate the technique used. Third, the NPC structure is only crudely identified in current experiments. For example, many experiments use Pom121 as a marker, but it is not known precisely where in the NPC structure this protein resides. As experimental precision improves and different nanoenvironments are elucidated, it will become critical to produce a precise position map of various proteins. Super-resolution techniques (for review see [67]) are expected to be useful for developing such a map. The major advantage of a light microscopy approach is that the measurements can be made in live, functioning NPCs, and can be directly correlated with single molecule transport trajectories in real-time. Finally, as spatial precision improves in super-fast imaging microscopy, movements of the NPC and NPC components will become more important. Accurate measurement of particle movement requires correlating movement with a precisely located reference object. If the reference object moves, this must be corrected, or the precision of the measurement suffers. Nanoscale movements of NPCs are more prevalent in live cells than permeabilized cells. Investigators in the motor protein field have been the leaders in developing precise measurements, and subnanometer accuracy is possible for multiple colors using active feedback [106].

In summary, single molecule studies of nucleocytoplasmic transport have provided unique insights on the properties of the NPC and the transport mechanism. The coming years promise further applications of existing technologies, as well as improved approaches that will allow us to address more difficult questions.

Acknowledgements

We thank Anton Zilman for critical evaluation of the manuscript. This work was supported by the NIH (GM065534 and GM084062), the DoD (N00014-02-1-0710), and the Welch Foundation (BE-1541).

Appendix A. Supplementary data

Supplementary data to this article can be found online at doi:10.1016/j.bbamcr.2010.12.011.

References

[1] K. Ribbeck, D. Görlich, Kinetic analysis of translocation through nuclear pore complexes, EMBO J. 20 (2001) 1320–1330.
[2] M.P. Rout, G. Blobel, Isolation of the yeast nuclear pore complex, J. Cell Biol. 123 (1993) 771–783.
[3] R. Reichelt, A. Holzenburg, J.E.L. Buhle, M. Jarnik, A. Engel, U. Aebi, Correlation between structure and mass distribution of the nuclear pore complex and of distinct pore complex components, J. Cell Biol. 110 (1990) 883–894.
[4] D. Stoffler, B. Feja, B. Fahrenkrog, J. Walz, D. Typke, U. Aebi, Cryo-electron tomography provides novel insights into nuclear pore architecture: implications for nucleocytoplasmic transport, J. Mol. Biol. 328 (2003) 119–130.
[5] N. Pante, M. Kann, Nuclear pore complex is able to transport macromolecules with diameters of about 39 nm, Mol. Biol. Cell 13 (2002) 425–434.
[6] B. Naim, D. Zbaida, S. Dagan, R. Kapon, Z. Reich, Cargo surface hydrophobicity is sufficient to overcome the nuclear pore complex selectivity barrier, EMBO J. 28 (2009) 2697–2705.
[7] L.J. Colwell, M.P. Brenner, K. Ribbeck, Charge as a selection criterion for translocation through the nuclear pore complex, PLoS Comput. Biol. 6 (2010) e1000747.
[8] L.J. Terry, S.R. Wente, Flexible gates: dynamic typologies and functions for FG nucleoporins in nucleocytoplasmic transport, Euk. Cell 8 (2009) 1814–1827.
[9] S.G. Brohawn, J.R. Partridge, J.R.R. Whittle, T.U. Schwartz, The nuclear pore complex has entered the atomic age, Structure 17 (2009) 1156–1168.
[10] R.Y.H. Lim, U. Aebi, B. Fahrenkrog, Towards reconciling structure and function in the nuclear pore complex, Histochem. Cell Biol. 129 (2008) 105–116.
[11] M. Stewart, Molecular mechanism of the nuclear protein import cycle, Nat. Rev. Mol. Cell Biol. 8 (2007) 195–208.
[12] J.M. Cronshaw, A.N. Krutchinsky, W. Zhang, B.T. Chait, M.J. Matunis, Proteomic analysis of the mammalian nuclear pore complex, J. Cell Biol. 158 (2002) 915–927.
[13] M.P. Rout, J.D. Aitchison, A. Suprapto, K. Hjertaas, Y. Zhao, B.T. Chait, The yeast nuclear pore complex: composition, architecture, and transport mechanism, J. Cell Biol. 148 (2000) 635–651.
[14] S.S. Patel, B.J. Belmont, J.M. Sante, M.F. Rexach, Natively unfolded nucleoporins gate protein diffusion across the nuclear pore complex, Cell 129 (2007) 83–96.
[15] D.P. Denning, M.F. Rexach, Rapid evolution exposes the boundaries of domain structure and function in natively unfolded FG nucleoporins, Mol. Cell. Proteomics 6 (2007) 272–282.
[16] V.V. Krishnan, E.Y. Lau, J. Yamada, D.P. Denning, S.S. Patel, M.E. Colvin, M.F. Rexach, Intramolecular cohesion of coils mediated by phenylalanine–glycine motifs in the natively unfolded domain of a nucleoporin, PLoS Comput. Biol. 4 (2008) e1000145.
[17] S. Frey, D. Görlich, A saturated FG-repeat hydrogel can reproduce the permeability properties of nuclear pore complexes, Cell 130 (2007) 512–523.
[18] R.Y. Lim, N.P. Huang, J. Koser, J. Deng, K.H. Lau, K. Schwarz-Herion, B. Fahrenkrog, U. Aebi, Flexible phenylalanine–glycine nucleoporins as entropic barriers to nucleocytoplasmic transport, Proc. Natl Acad. Sci. USA 103 (2006) 9512–9517.
[19] I.G. Macara, Transport into and out of the nucleus, Microbiol. Mol. Biol. Rev. 65 (2001) 570–594.
[20] W. Yang, J. Gelles, S.M. Musser, Imaging of single-molecule translocation through nuclear pore complexes, Proc. Natl Acad. Sci. USA 101 (2004) 12887–12892.
[21] W. Yang, S.M. Musser, Nuclear import time and transport efficiency depend on importin beta concentration, J. Cell Biol. 174 (2006) 951–961.
[22] H. Fried, U. Kutay, Nucleocytoplasmic transport: taking an inventory, Cell. Mol. Life Sci. 60 (2003) 1659–1688.
[23] D. Görlich, U. Kutay, Transport between the cell nucleus and the cytoplasm, Annu. Rev. Cell Dev. Biol. 15 (1999) 607–660.
[24] R.Y. Lim, K.S. Ullman, B. Fahrenkrog, Biology and biophysics of the nuclear pore complex and its components, Int. Rev. Cell Mol. Biol. 267 (2008) 299–342.
[25] R. Peters, Functionalization of a nanopore: the nuclear pore complex paradigm, Biochim. Biophys. Acta 1793 (2009) 1533–1539.
[26] E.J. Tran, S.R. Wente, Dynamic nuclear pore complexes: life on the edge, Cell 125 (2006) 1041–1053.
[27] S. Frey, D. Görlich, FG/FxFG as well as GLFG repeats form a selective permeability barrier with self-healing properties, EMBO J. 28 (2009) 2554–2567.
[28] B. Naim, V. Brumfeld, R. Kapon, V. Kiss, R. Nevo, Z. Reich, Passive and facilitated transport in nuclear pore complexes is largely uncoupled, J. Biol. Chem. 282 (2007) 3881–3888.
[29] L.M. McLane, A.H. Corbett, Nuclear localization signals and human disease, IUBMB Life 61 (2009) 697–706.
[30] D.A. Mason, D.E. Stage, D.S. Goldfarb, Evolution of the metazoan-specific importin alpha gene family, J. Mol. Evol. 68 (2009) 351–365.
[31] J. Tejomurtula, K.B. Lee, S.K. Tripurani, G.W. Smith, J. Yao, Role of importin alpha8, a new member of the importin alpha family of nuclear transport proteins, in early embryonic development in cattle, Biol. Reprod. 81 (2009) 333–342.
[32] P. Askjaer, T.H. Jensen, J. Nilsson, L. Englmeier, J. Kjems, The specificity of the CRM1-Rev nuclear export signal interaction is mediated by RanGTP, J. Biol. Chem. 273 (1998) 33414–33422.
[33] E. Paraskeva, E. Izaurralde, F.R. Bischoff, J. Huber, U. Kutay, E. Hartmann, R. Luhrmann, D. Görlich, CRM1-mediated recycling of snurportin 1 to the cytoplasm, J. Cell Biol. 145 (1999) 255–264.
[34] N.R. Yaseen, G. Blobel, GTP hydrolysis links initiation and termination of nuclear import on the nucleoporin Nup358, J. Biol. Chem. 274 (1999) 26493–26502.
[35] M. Floer, G. Blobel, Putative reaction intermediates in Crm1-mediated nuclear protein export, J. Biol. Chem. 274 (1999) 16279–16286.
[36] M. Floer, G. Blobel, M. Rexach, Disassembly of RanGTP–karyopherin β complex, an intermediate in nuclear protein import, J. Biol. Chem. 272 (1997) 19538–19546.
[37] F.R. Bischoff, D. Görlich, RanBP1 is crucial for the release of RanGTP from importin β-related nuclear transport factors, FEBS Lett. 419 (1997) 249–254.
[38] K. Ribbeck, G. Lipowsky, H.M. Kent, M. Stewart, D. Görlich, NTF2 mediates nuclear import of Ran, EMBO J. 17 (1998) 6587–6598.
[39] Y. Matsuura, M. Stewart, Nup50/Npap60 function in nuclear protein import complex disassembly and importin recycling, EMBO J. 24 (2005) 3681–3689.
[40] C. Sun, W. Yang, L.C. Tu, S.M. Musser, Single-molecule measurements of importin alpha/cargo complex dissociation at the nuclear pore, Proc. Natl Acad. Sci. USA 105 (2008) 8613–8618.
[41] D. Gilchrist, B. Mykytka, M. Rexach, Accelerating the rate of disassembly of karyopherin·cargo complexes, J. Biol. Chem. 277 (2002) 18161–18172.
[42] D. Gilchrist, M. Rexach, Molecular basis for the rapid dissociation of nuclear localization signals from karyopherin α in the nucleoplasm, J. Biol. Chem. 278 (2003) 51937–51949.
[43] S. Hutten, A. Flotho, F. Melchior, R.H. Kehlenbach, The Nup358–RanGAP complex is required for efficient importin alpha/beta-dependent nuclear import, Mol. Biol. Cell 19 (2008) 2300–2310.
[44] S. Hutten, S. Walde, C. Spillner, J. Hauber, R.H. Kehlenbach, The nuclear pore component Nup358 promotes transportin-dependent nuclear import, J. Cell Sci. 122 (2009) 1100–1110.
[45] D. Görlich, M.J. Seewald, K. Ribbeck, Characterization of Ran-driven cargo transport and the RanGTPase system by kinetic measurements and computer simulation, EMBO J. 22 (2003) 1088–1100.
[46] M.V. Nachury, K. Weis, The direction of transport through the nuclear pore can be inverted, Proc. Natl Acad. Sci. USA 96 (1999) 9622–9627.
[47] D. Grünwald, A. Hoekstra, T. Dange, V. Buschmann, U. Kubitscheck, Direct observation of single protein molecules in aqueous solution, Chemphyschem 7 (2006) 812–815.
[48] T. Dange, D. Grünwald, A. Grünwald, R. Peters, U. Kubitscheck, Autonomy and robustness of translocation through the nuclear pore complex: a single-molecule study, J. Cell Biol. 183 (2008) 77–86.
[49] U. Kubitscheck, D. Grünwald, A. Hoekstra, D. Rohleder, T. Kues, J.P. Siebrasse, R. Peters, Nuclear transport of single molecules: dwell times at the nuclear pore complex, J. Cell Biol. 168 (2005) 233–243.
[50] W. Yang, S.M. Musser, Visualizing single molecules interacting with nuclear pore complexes by narrow-field epifluorescence microscopy, Methods 39 (2006) 316–328.
[51] N. Daigle, J. Beaudouin, L. Hartnell, G. Imreh, E. Hallberg, J. Lippincott-Schwartz, J. Ellenberg, Nuclear pore complexes form immobile networks and have a very low turnover in live mammalian cells, J. Cell Biol. 154 (2001) 71–84.
[52] E. Lang, J. Baier, J. Kohler, Epifluorescence, confocal and total internal reflection microscopy for single-molecule experiments: a quantitative comparison, J. Microsc. 222 (2006) 118–123.
[53] T. Schmidt, G.J. Schutz, W. Baumgartner, H.J. Gruber, H. Schindler, Imaging of single molecule diffusion, Proc. Natl Acad. Sci. USA 93 (1996) 2926–2929.
[54] J. Peter, U. Kubitscheck, Single molecule tracking for studying nucleocytoplasmic transport and intranuclear dynamics, in: R. Hancock (Ed.), The Nucleus, vol. 2, Humana, Totowa, N.J., 2008, pp. 343–361.
[55] M. Tokunaga, N. Imamoto, K. Sakata-Sogawa, Highly inclined thin illumination enables clear single-molecule imaging in cells, Nat. Meth. 5 (2008) 159–161.
[56] J. Ma, W. Yang, Three-dimensional distribution of transient interactions in the nuclear pore complex obtained from single-molecule snapshots, Proc. Natl Acad. Sci. USA 107 (2010) 7305–7310.
[57] R.N. Day, M.W. Davidson, The fluorescent protein palette: tools for cellular imaging, Chem. Soc. Rev. 38 (2009) 2887–2921.
[58] D.M. Leslie, B. Timney, M.P. Rout, J.D. Aitchison, Studying nuclear protein import in yeast, Methods 39 (2006) 291–308.
[59] M. Bucci, S.R. Wente, *In vivo* dynamics of nuclear pore complexes in yeast, J. Cell Biol. 136 (1997) 1185–1199.
[60] S.A. Adam, R.S. Marr, L. Gerace, Nuclear protein import in permeabilized mammalian cells requires soluble cytoplasmic factors, J. Cell Biol. 111 (1990) 807–816.
[61] D. Görlich, S. Prehn, R.A. Laskey, E. Hartmann, Isolation of a protein that is essential for the first step of nuclear protein import, Cell 79 (1994) 767–778.
[62] E.J.H. Adam, S.A. Adam, Identification of cytosolic factors required for nuclear location sequence-mediated binding to the nuclear envelope, J. Cell Biol. 125 (1994) 547–555.
[63] F. Melchior, B.M. Paschal, J. Evans, L. Gerace, Inhibition of nuclear protein import by nonhydrolyzable analogues of GTP and identification of the small GTPase Ran/TC4 as an essential transport factor, J. Cell Biol. 123 (1993) 1649–1659.
[64] M.S. Moore, G. Blobel, The GTP-binding protein Tan/TC4 is required for protein import into the nucleus, Nature 365 (1993) 661–663.
[65] R.H. Kehlenbach, *In vitro* analysis of nuclear mRNA export using molecular beacons for target detection, Nucleic Acids Res. 31 (2003) e64.
[66] D. Grünwald, R.H. Singer, *In vivo* imaging of labelled endogeneous β-actin mRNA during nucleocytoplasmic transport, Nature 467 (2010) 604–607.

[67] B. Huang, M. Bates, X. Zhuang, Super-resolution fluorescence microscopy, Annu. Rev. Biochem. 78 (2009) 993–1016.
[68] A. Yildiz, J.N. Forkey, S.A. McKinney, T. Ha, Y.E. Goldman, P.R. Selvin, Myosin V walks hand-over-hand: single fluorophore imaging with 1.5-nm localization, Science 300 (2003) 2061–2065.
[69] M. Kahms, P. Lehrich, J. Huve, N. Sanetra, R. Peters, Binding site distribution of nuclear transport receptors and transport complexes in single nuclear pore complexes, Traffic 10 (2009) 1228–1242.
[70] A.R. Lowe, J.J. Siegel, P. Kalab, M. Siu, K. Weis, J.T. Liphardt, Selectivity mechanism of the nuclear pore complex characterized by single cargo tracking, Nature 467 (2010) 600–603.
[71] C. Joo, H. Balci, Y. Ishitsuka, C. Buranachai, T. Ha, Advances in single-molecule fluorescence methods for molecular biology, Annu. Rev. Biochem. 77 (2008) 51–76.
[72] S.R. Carmody, S.R. Wente, mRNA nuclear export at a glance, J. Cell Sci. 122 (2009) 1933–1937.
[73] A. Zilman, J. Pearson, G. Bel, Effects of jamming on nonequilibrium transport times in nanochannels, Phys. Rev. Lett. 103 (2009) 128103.
[74] D. Görlich, N. Pante, U. Kutay, U. Aebi, F.R. Bischoff, Identification of different roles for RanGDP and RanGTP in nuclear protein import, EMBO J. 15 (1996) 5584–5594.
[75] A. Zilman, Effects of multiple occupancy and interparticle interactions on selective transport through narrow channels: theory versus experiment, Biophys. J. 96 (2009) 1235–1248.
[76] A. Zilman, S. Di Talia, B.T. Chait, M.P. Rout, M.O. Magnasco, Efficiency, selectivity, and robustness of nucleocytoplasmic transport, PLoS Comput. Biol. 3 (2007) e125.
[77] A. Zilman, S. Di Talia, T. Jovanovic-Talisman, B.T. Chait, M.P. Rout, M.O. Magnasco, Enhancement of transport selectivity through nano-channels by non-specific competition, PLoS Comp. Biol. 6 (2010) e1000804.
[78] M. Rexach, G. Blobel, Protein import into nuclei: association and dissociation reactions involving transport substrate, transport factors, and nucleoporins, Cell 83 (1995) 683–692.
[79] U. Kutay, F.R. Bischoff, S. Kostka, R. Kraft, D. Görlich, Export of importin α from the nucleus is mediated by a specific nuclear transport factor, Cell 90 (1997) 1061–1071.
[80] T. Jovanovic-Talisman, J. Tetenbaum-Novatt, A.S. McKenney, A. Zilman, R. Peters, M.P. Rout, B.T. Chait, Artificial nanopores that mimic the transport selectivity of the nuclear pore complex, Nature 457 (2009) 1023–1027.
[81] D. Mohr, S. Frey, T. Fischer, T. Guttler, D. Görlich, Characterisation of the passive permeability barrier of nuclear pore complexes, EMBO J. 28 (2009) 2541–2553.
[82] I. Zemp, U. Kutay, Nuclear export and cytoplasmic maturation of ribosomal subunits, FEBS Lett. 581 (2007) 2783–2793.
[83] A.E. Smith, A. Helenius, How viruses enter animal cells, Science 304 (2004) 237–242.
[84] R. Kapon, A. Topchik, D. Mukamel, Z. Reich, A possible mechanism for self-coordination of bidirectional traffic across nuclear pores, Phys. Biol. 5 (2008) 036001.
[85] J. Yamada, J.L. Phillips, S. Patel, G. Goldfien, A. Calestagne-Morelli, H. Huang, R. Rexza, J. Acheson, V.V. Krishnan, S. Newsam, A. Gopinathan, E.Y. Lau, M.E. Colvin, V.N. Uversky, M.F. Rexach, A bimodal distribution of two distinct categories of intrinsically-disordered structures with separate functions in FG nucleoporins, Mol. Cell. Proteomics 9 (2010) 2205–2224.
[86] D.P. Denning, S.S. Patel, V. Uversky, A.L. Fink, M. Rexach, Disorder in the nuclear pore complex: the FG repeat regions of nucleoporins are natively unfolded, Proc. Natl Acad. Sci. USA 100 (2003) 2450–2455.
[87] P.-G. de Gennes, Scaling Concepts in Polymer Physics, Cornell University Press, Ithaca, N.Y., 1979.
[88] P.-G. de Gennes, Polymers at an interface; a simplified view, Adv. Colloid Int. Sci. 27 (1987) 189–209.
[89] S. Frey, R.P. Richter, D. Görlich, FG-rich repeats of nuclear pore proteins form a three-dimensional meshwork with hydrogel-like properties, Science 314 (2006) 815–817.
[90] C. Ader, S. Frey, W. Maas, H.B. Schmidt, D. Görlich, M. Baldus, Amyloid-like interactions within nucleoporin FG hydrogels, Proc. Natl Acad. Sci. USA 107 (2010) 6281–6285.
[91] L.A. Strawn, T. Shen, N. Shulga, D.S. Goldfarb, S.R. Wente, Minimal nuclear pore complexes define FG repeat domains essential for transport, Nat. Cell Biol. 6 (2004) 197–206.
[92] A. Abu-Arish, P. Kalab, J. Ng-Kamstra, K. Weis, C. Fradin, Spatial distribution and mobility of the Ran GTPase in live interphase cells, Biophys. J. 97 (2009) 2164–2178.
[93] M. Rhee, M.A. Burns, Nanopore sequencing technology: nanopore preparations, Trends Biotechnol. 25 (2007) 174–181.
[94] R.Y. Lim, B. Fahrenkrog, J. Koser, K. Schwarz-Herion, J. Deng, U. Aebi, Nanomechanical basis of selective gating by the nuclear pore complex, Science 318 (2007) 640–643.
[95] R. Bayliss, T. Littlewood, M. Stewart, Structural basis for the interaction between FxFG nucleoporin repeats and importin-beta in nuclear trafficking, Cell 102 (2000) 99–108.
[96] R. Bayliss, T. Littlewood, L.A. Strawn, S.R. Wente, M. Stewart, GLFG and FxFG nucleoporins bind to overlapping sites on importin-beta, J. Biol. Chem. 277 (2002) 50597–50606.
[97] J. Bednenko, G. Cingolani, L. Gerace, Importin beta contains a COOH-terminal nucleoporin binding region important for nuclear transport, J. Cell Biol. 162 (2003) 391–401.
[98] T.A. Isgro, K. Schulten, Binding dynamics of isolated nucleoporin repeat regions to importin-beta, Structure 13 (2005) 1869–1879.
[99] S.M. Liu, M. Stewart, Structural basis for the high-affinity binding of nucleoporin Nup1p to the *Saccharomyces cerevisiae* importin-beta homologue, Kap95p, J. Mol. Biol. 349 (2005) 515–525.
[100] K. Luby-Phelps, Cytoarchitecture and physical properties of cytoplasm: volume, viscosity, diffusion, intracellular surface area, Int. Rev. Cytol. 192 (2000) 189–221.
[101] J. Fiserova, S.A. Richards, S.R. Wente, M.W. Goldberg, Facilited transport and diffusion take distinct spatial routes through the nuclear pore complex, J. Cell Sci. 123 (2010) 2773–2780.
[102] L. Holtzer, T. Meckel, T. Schmidt, Nanometric three-dimensional tracking of individual quantum dots in cells, Appl. Phys. Lett. 90 (2007) 053902.
[103] P. Prabhat, S. Ram, E.S. Ward, R.J. Ober, Simultaneous imaging of different focal planes in fluorescence microscopy for the study of cellular dynamics in three dimensions, IEEE Trans. Nanobioscience 3 (2004) 237–242.
[104] E. Toprak, H. Balci, B.H. Blehm, P.R. Selvin, Three-dimensional particle tracking via bifocal imaging, Nano Lett. 7 (2007) 2043–2045.
[105] N.P. Wells, G.A. Lessard, J.H. Werner, Confocal, three-dimensional tracking of individual quantum dots in high-background environments, Anal. Chem. 80 (2008) 9830–9834.
[106] A. Pertsinidis, Y. Zhang, S. Chu, Subnanometre single-molecule localization, registration and distance measurements, Nature 466 (2010) 647–651.
[107] C. Chaillan-Huntington, P.J.G. Butler, J.A. Huntington, D. Akin, C. Feldherr, M. Stewart, NTF2 monomer-dimer equilibrium, J. Mol. Biol. 314 (2001) 465–477.
[108] C.W. Akey, M. Radermacher, Architecture of the Xenopus nuclear pore complex revealed by three-dimensional cryo-electron microscopy, J. Cell Biol. 122 (1993) 1–19.
[109] M. Jarnik, U. Aebi, Toward a more complete 3-D structure of the nuclear pore complex, J. Struct. Biol. 107 (1991) 291–308.
[110] J.E. Hinshaw, B.O. Carragher, R.A. Milligan, Architecture and design of the nuclear pore complex, Cell 69 (1992) 1133–1141.
[111] D. Frenkiel-Krispin, B. Maco, U. Aebi, O. Medalia, Structural analysis of a metazoan nuclear pore complex reveals a fused concentric ring architecture, J. Mol. Biol. 395 (2010) 578–586.

SUPPLEMENTARY DATA

SIMPLE DIFFUSION MODEL

This section elaborates on the simple diffusion model described by Frey and Görlich [1] and similarly derived by Zilman and coworkers [2, 3]. The basic model was described in the main text (Figure 6 and equation 1). We note that fluxes calculated from the true kinetic rate constants, k_{in} and k_{out}, require multiplication by δ, which is a microscopic length corresponding to the width of the transition region [4]. To make the math easier, Frey and Görlich [1] include δ in their rate constants, i.e., $k_1 = k_{in}\delta$ and $k_{-1} = k_{out}\delta$ (see Figure 6A), which thus have units of length/s. This becomes important for the derivation of transport efficiency.

As Frey and Görlich described earlier [1], if a steady-state condition is assumed, the concentration gradient within the pore must be linear (dC/dx is constant over the permeability barrier), according to Fick's first law [5] and since the potential energy surface is flat (Figure 6). Under these conditions, the flux, J, of particles crossing the area, A, each second is the same across the pore, at each pore exit and within the pore itself:

$$J_{C\Rightarrow BC} = J_{BC\Rightarrow BN} = J_{BN\Rightarrow N} = J_{C\Rightarrow N} = J \qquad \text{(eq. S1)}$$

$$J_{C\Rightarrow BC} = A(k_1 C_C - k_{-1} C_{BC}) \qquad \text{(eq. S2)}$$

$$J_{BC\Rightarrow BN} = -\frac{AD}{L}(C_{BN} - C_{BC}) \qquad \text{(eq. S3)}$$

$$J_{BN\Rightarrow N} = A(k_{-1} C_{BN} - k_1 C_N) \qquad \text{(eq. S4)}$$

where D is the diffusion constant within the pore and L is the length of the pore. Solving eqs. S2 and S4 for C_{BC} and C_{BN}, respectively, and then substituting into eq. S3 yields eq. 2. Note that a positive flux according to Frey and Görlich [1] describes efflux from the nucleus. We have corrected this here so that a positive flux represents import into the nucleus.

Under the non-equilibrium steady-state condition where $C_C > C_N$, there is net particle movement into the nucleus, which implies that C_{BC} and C_{BN} are less than and greater than, respectively, the concentrations predicted by the equilibrium conditions. Therefore,

$$\alpha K = \frac{C_{BC}}{C_C} \quad \text{and} \quad \beta K = \frac{C_{BN}}{C_N} \qquad \text{(eqs. S5a and S5b)}$$

where the coefficients α (< 1) and β (> 1) depend on the C_C/C_N ratio. Setting eqs. S2 and S4 equal to each other and using eqs. S5a and S5b to simplify yields:

$$\frac{C_C}{C_N} = \frac{\beta - 1}{1 - \alpha} \qquad \text{(eq. S6)}$$

Setting eqs. 2 and S3 equal to each other, eliminating C_{BN} and C_{BC} with eqs. S5a and S5b, and then eliminating β with eq. S6 yields α:

$$\alpha = \frac{1}{2}\left[\left(1+\frac{C_N}{C_C}\right)+\left(1-\frac{C_N}{C_C}\right)\left(\frac{\gamma}{\gamma+1}\right)\right] \qquad \text{(eq. S7)}$$

The minimum for α is 0.5 (γ << 1 and high C_C/C_N ratio) and the maximum is 1 (γ >> 1 or C_C/C_N = 1) (Figure S1A). Eqs. S6 and S7 yield β:

$$\beta = \frac{1}{2}\left[\left(1+\frac{C_C}{C_N}\right)+\left(1-\frac{C_C}{C_N}\right)\left(\frac{\gamma}{\gamma+1}\right)\right] \qquad \text{(eq. S8)}$$

The minimum for β is 1 (γ >> 1 or C_C/C_N = 1) (Figure S1B). From eqs. S5a and S5b,

$$\frac{C_{BC}}{C_{BN}} = \frac{\alpha}{\beta}\frac{C_C}{C_N} \qquad \text{(eq. S9)}$$

According to the hydrogel results of Frey and Görlich [1, 6], γ is typically less than 0.05 for facilitated transport. Thus, $C_{BC}/C_{BN} \approx 1$ (Figure S2). As a reminder, at the single molecule and single pore level, concentrations are unsuitable variables. Instead, probabilities are more appropriate. However, concentration ratios are equivalent to probability ratios.

As defined in the text, the transport efficiency, E, is the number of particles that exit into the nucleus divided by the total number of particles that enter the pore from the cytoplasm. Thus, E is the probability for transit after a particle first enters the pore. The total input flux to the pore from the cytoplasm is Ak_1C_C. Therefore, the total import flux to the nucleoplasm that originates in the cytoplasm is EAk_1C_C. Due to symmetry, the total export flux to the cytoplasm that originates in the nucleoplasm is EAk_1C_N. The total import flux to the nucleoplasm that originates in the nucleoplasm (enters the pore from the nucleus and aborts transport) is $(1\text{-}E)Ak_1C_N$. The total nuclear exit flux includes molecules that enter the pore from the cytoplasm and the nucleoplasm:

$$Ak_{-1}C_{BN} = AEk_1C_C + A\left(1-E\right)k_1C_N \qquad \text{(eq. S10)}$$

A similar equation can be written for the export flux. Solving for E using eqs. S5b and S8 yields:

$$E = \frac{1}{2\left(\gamma+1\right)} = \frac{1}{\frac{Lk_{-1}}{D}+2} \qquad \text{(eq. S11)}$$

which is provided in the main text as equation 4. Assuming $k_{out} \approx (D_\delta/\delta^2)e^{-u}$, where δ is the approximate length of the transition region and D_δ is the diffusion constant in this region [4], then $k_{-1} \approx (D/\delta)e^{-u}$ and:

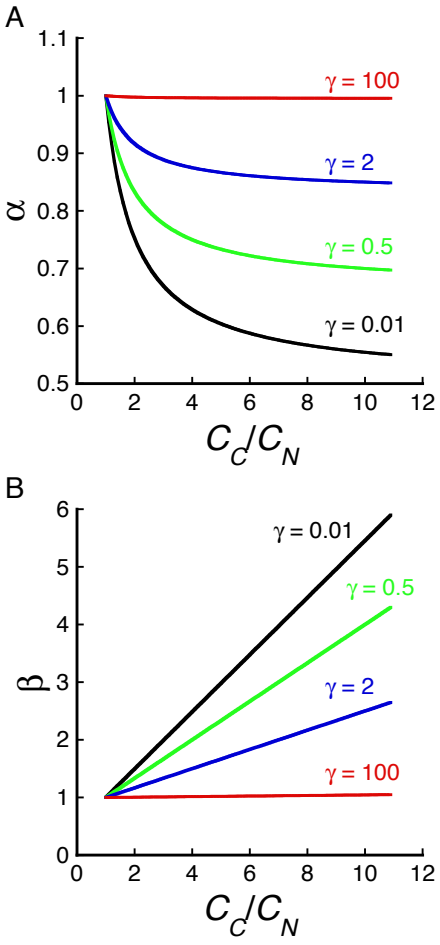

Figure S1. α and β Dependence on the C_C/C_N Ratio. α [= $(1/K)(C_{BC}/C_C)$] and β [= $(1/K)(C_{BN}/C_N)$] measure how the concentration ratios at the exit interfaces differ from their equilibrium values, and are calculated according to equations S7 and S8. α and β are both 1 at equilibrium. See text for details.

$$E \approx \frac{1}{\frac{LD_\delta}{\delta D} e^{-u} + 2} \qquad \text{(eq. S12)}$$

A similar result was derived and later modified by Zilman and coworkers [2, 3]. In their analysis, a constant ($4/\pi$) is multiplied by the first term in the denominator to account for the circular opening to the channel [2]. As discussed in the main text, Zilman and coworkers distinguish between 'transport efficiency' and 'translocation probability' (the latter of which is E as defined here). To convert E as defined here to the 'transport efficiency' as defined by Zilman and coworkers, the incoming flux (Ak_1C_C) should be multiplied by a probability that the particle actually enters the channel, rather than is rejected due to lack of space.

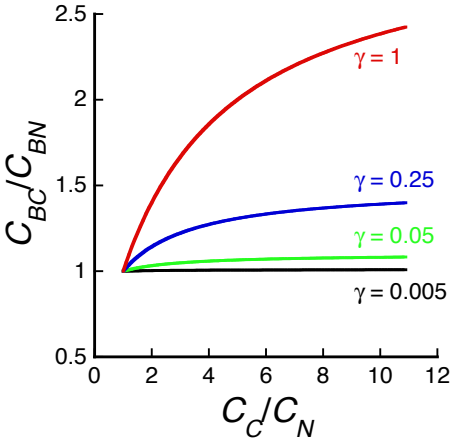

Figure S2. C_{BC}/C_{BN} Dependence on the C_C/C_N Ratio. Concentration variations within the pore due to diffusion gradients are predicted to be low. C_{BC}/C_{BN} ratios are calculated according to equation S9. See text for details.

References

[1] S. Frey, D. Görlich, A saturated FG-repeat hydrogel can reproduce the permeability properties of nuclear pore complexes, Cell 130 (2007) 512-523.

[2] A. Zilman, Effects of multiple occupancy and interparticle interactions on selective transport through narrow channels: theory versus experiment, Biophys J 96 (2009) 1235-1248.

[3] A. Zilman, S. Di Talia, B.T. Chait, M.P. Rout, M.O. Magnasco, Efficiency, selectivity, and robustness of nucleocytoplasmic transport, PLoS Comput Biol 3 (2007) e125.

[4] T. Bickel, R. Bruinsma, The nuclear pore complex mystery and anomalous diffusion in reversible gels, Biophys J 83 (2002) 3079-3087.

[5] H.C. Berg, Random Walks in Biology, Princeton University Press, Princeton, NJ, 1993.

[6] S. Frey, D. Görlich, FG/FxFG as well as GLFG repeats form a selective permeability barrier with self-healing properties, EMBO J 28 (2009) 2554-2567.

SUPPLEMENTARY DATA

SIMPLE DIFFUSION MODEL

This section elaborates on the simple diffusion model described by Frey and Görlich [1] and similarly derived by Zilman and coworkers [2, 3]. The basic model was described in the main text (Figure 6 and equation 1). We note that fluxes calculated from the true kinetic rate constants, k_{in} and k_{out}, require multiplication by δ, which is a microscopic length corresponding to the width of the transition region [4]. To make the math easier, Frey and Görlich [1] include δ in their rate constants, i.e., $k_1 = k_{in}\delta$ and $k_{-1} = k_{out}\delta$ (see Figure 6A), which thus have units of length/s. This becomes important for the derivation of transport efficiency.

As Frey and Görlich described earlier [1], if a steady-state condition is assumed, the concentration gradient within the pore must be linear (dC/dx is constant over the permeability barrier), according to Fick's first law [5] and since the potential energy surface is flat (Figure 6). Under these conditions, the flux, J, of particles crossing the area, A, each second is the same across the pore, at each pore exit and within the pore itself:

$$J_{C\Rightarrow BC} = J_{BC\Rightarrow BN} = J_{BN\Rightarrow N} = J_{C\Rightarrow N} = J \qquad \text{(eq. S1)}$$

$$J_{C\Rightarrow BC} = A(k_1 C_C - k_{-1} C_{BC}) \qquad \text{(eq. S2)}$$

$$J_{BC\Rightarrow BN} = -\frac{AD}{L}(C_{BN} - C_{BC}) \qquad \text{(eq. S3)}$$

$$J_{BN\Rightarrow N} = A(k_{-1} C_{BN} - k_1 C_N) \qquad \text{(eq. S4)}$$

where D is the diffusion constant within the pore and L is the length of the pore. Solving eqs. S2 and S4 for C_{BC} and C_{BN}, respectively, and then substituting into eq. S3 yields eq. 2. Note that a positive flux according to Frey and Görlich [1] describes efflux from the nucleus. We have corrected this here so that a positive flux represents import into the nucleus.

Under the non-equilibrium steady-state condition where $C_C > C_N$, there is net particle movement into the nucleus, which implies that C_{BC} and C_{BN} are less than and greater than, respectively, the concentrations predicted by the equilibrium conditions. Therefore,

$$\alpha K = \frac{C_{BC}}{C_C} \quad \text{and} \quad \beta K = \frac{C_{BN}}{C_N} \qquad \text{(eqs. S5a and S5b)}$$

where the coefficients α (< 1) and β (> 1) depend on the C_C/C_N ratio. Setting eqs. S2 and S4 equal to each other and using eqs. S5a and S5b to simplify yields:

$$\frac{C_C}{C_N} = \frac{\beta - 1}{1 - \alpha} \qquad \text{(eq. S6)}$$

Setting eqs. 2 and S3 equal to each other, eliminating C_{BN} and C_{BC} with eqs. S5a and S5b, and then eliminating β with eq. S6 yields α:

$$\alpha = \frac{1}{2}\left[\left(1+\frac{C_N}{C_C}\right)+\left(1-\frac{C_N}{C_C}\right)\left(\frac{\gamma}{\gamma+1}\right)\right] \qquad \text{(eq. S7)}$$

The minimum for α is 0.5 (γ << 1 and high C_C/C_N ratio) and the maximum is 1 (γ >> 1 or C_C/C_N = 1) (Figure S1A). Eqs. S6 and S7 yield β:

$$\beta = \frac{1}{2}\left[\left(1+\frac{C_C}{C_N}\right)+\left(1-\frac{C_C}{C_N}\right)\left(\frac{\gamma}{\gamma+1}\right)\right] \qquad \text{(eq. S8)}$$

The minimum for β is 1 (γ >> 1 or C_C/C_N = 1) (Figure S1B). From eqs. S5a and S5b,

$$\frac{C_{BC}}{C_{BN}} = \frac{\alpha}{\beta}\frac{C_C}{C_N} \qquad \text{(eq. S9)}$$

According to the hydrogel results of Frey and Görlich [1, 6], γ is typically less than 0.05 for facilitated transport. Thus, $C_{BC}/C_{BN} \approx 1$ (Figure S2). As a reminder, at the single molecule and single pore level, concentrations are unsuitable variables. Instead, probabilities are more appropriate. However, concentration ratios are equivalent to probability ratios.

As defined in the text, the transport efficiency, E, is the number of particles that exit into the nucleus divided by the total number of particles that enter the pore from the cytoplasm. Thus, E is the probability for transit after a particle first enters the pore. The total input flux to the pore from the cytoplasm is Ak_1C_C. Therefore, the total import flux to the nucleoplasm that originates in the cytoplasm is EAk_1C_C. Due to symmetry, the total export flux to the cytoplasm that originates in the nucleoplasm is EAk_1C_N. The total import flux to the nucleoplasm that originates in the nucleoplasm (enters the pore from the nucleus and aborts transport) is $(1\text{-}E)Ak_1C_N$. The total nuclear exit flux includes molecules that enter the pore from the cytoplasm and the nucleoplasm:

$$Ak_{-1}C_{BN} = AEk_1C_C + A\left(1-E\right)k_1C_N \qquad \text{(eq. S10)}$$

A similar equation can be written for the export flux. Solving for E using eqs. S5b and S8 yields:

$$E = \frac{1}{2\left(\gamma+1\right)} = \frac{1}{\frac{Lk_{-1}}{D}+2} \qquad \text{(eq. S11)}$$

which is provided in the main text as equation 4. Assuming $k_{out} \approx (D_\delta/\delta^2)e^{-u}$, where δ is the approximate length of the transition region and D_δ is the diffusion constant in this region [4], then $k_{-1} \approx (D/\delta)e^{-u}$ and:

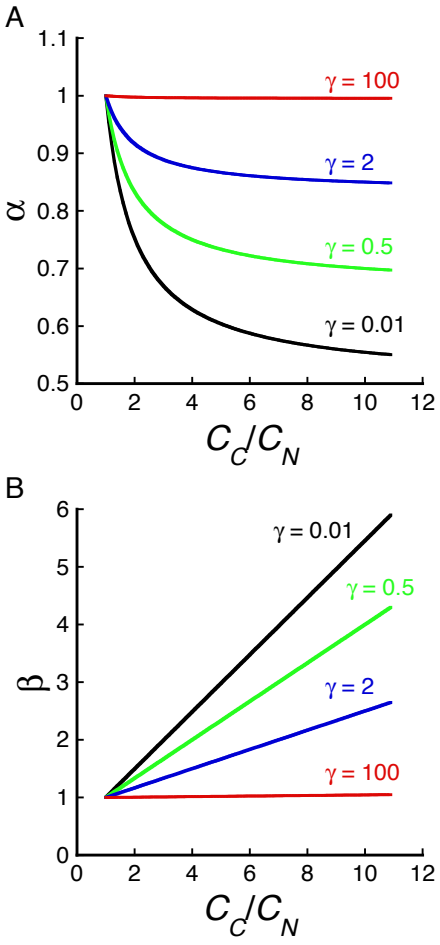

Figure S1. α and β Dependence on the C_C/C_N Ratio. α [= $(1/K)(C_{BC}/C_C)$] and β [= $(1/K)(C_{BN}/C_N)$] measure how the concentration ratios at the exit interfaces differ from their equilibrium values, and are calculated according to equations S7 and S8. α and β are both 1 at equilibrium. See text for details.

$$E \approx \frac{1}{\frac{LD_\delta}{\delta D} e^{-u} + 2} \qquad \text{(eq. S12)}$$

A similar result was derived and later modified by Zilman and coworkers [2, 3]. In their analysis, a constant ($4/\pi$) is multiplied by the first term in the denominator to account for the circular opening to the channel [2]. As discussed in the main text, Zilman and coworkers distinguish between 'transport efficiency' and 'translocation probability' (the latter of which is E as defined here). To convert E as defined here to the 'transport efficiency' as defined by Zilman and coworkers, the incoming flux (Ak_1C_C) should be multiplied by a probability that the particle actually enters the channel, rather than is rejected due to lack of space.

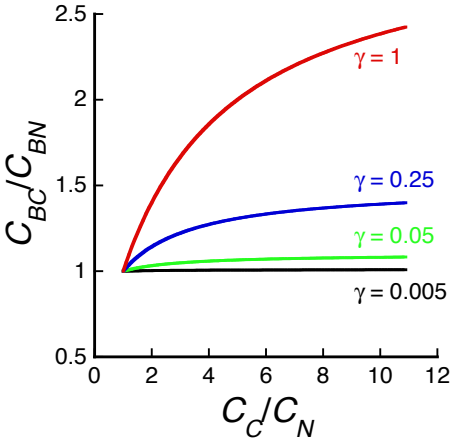

Figure S2. C_{BC}/C_{BN} Dependence on the C_C/C_N Ratio. Concentration variations within the pore due to diffusion gradients are predicted to be low. C_{BC}/C_{BN} ratios are calculated according to equation S9. See text for details.

References

[1] S. Frey, D. Görlich, A saturated FG-repeat hydrogel can reproduce the permeability properties of nuclear pore complexes, Cell 130 (2007) 512-523.

[2] A. Zilman, Effects of multiple occupancy and interparticle interactions on selective transport through narrow channels: theory versus experiment, Biophys J 96 (2009) 1235-1248.

[3] A. Zilman, S. Di Talia, B.T. Chait, M.P. Rout, M.O. Magnasco, Efficiency, selectivity, and robustness of nucleocytoplasmic transport, PLoS Comput Biol 3 (2007) e125.

[4] T. Bickel, R. Bruinsma, The nuclear pore complex mystery and anomalous diffusion in reversible gels, Biophys J 83 (2002) 3079-3087.

[5] H.C. Berg, Random Walks in Biology, Princeton University Press, Princeton, NJ, 1993.

[6] S. Frey, D. Görlich, FG/FxFG as well as GLFG repeats form a selective permeability barrier with self-healing properties, EMBO J 28 (2009) 2554-2567.